2009

A New ZCS-PWM Full-Bridge Boost Converter

Ahmad Mousavi

A New ZCS-PWM Full-Bridge Boost Converter

(Thesis Format: Monograph)

by

Ahmad Mousavi

Faculty of Engineering
Department of Electrical and Computer Engineering
Graduate Program in Engineering Science

A thesis submitted in partial fulfillment
of the requirements for the degree of
Master of Engineering Science

School of Graduate and Postdoctoral Studies
The University of Western Ontario
London, Ontario, Canada

ABSTRACT

The objective of this thesis is to propose, analyze, design, implement, and experimentally confirm the operation of a new Zero-Current-Switching PWM dc-dc full-bridge boost converter that does not have the drawbacks of previously proposed circuits of the same type. In this thesis, the general operating principles of the converter are reviewed, and the converter's operation is discussed in detail and analyzed mathematically. As a result of the mathematical analysis, key voltage and current equations that describes the operation of the auxiliary circuit and other converter devices have been derived. The steady state equations of each mode of operation are used as the basis of a MATLAB program that is used to generate steady-state characteristic curves that shows the effect that individual circuit parameters have on the operation of the auxiliary circuit and the boost converter.

Observations as to their steady-state characteristics are made and the curves are used as part of a design procedure to select the components of the converter, especially those of the auxiliary circuit. An experimental full-bridge PWM dc-dc boost converter prototype is built based on the converter design and typical waveforms are presented. The efficiency of the proposed converter operating with the auxiliary circuit is compared to that of a standard PWM dc-dc full-bridge boost converter and the increased efficiency of the proposed converter is confirmed.

ACKNOWLEDGEMENTS

I wish to express my most sincere gratitude to my supervisor Dr. G. Moschopoulos under whose supervision this Masters dissertation was conducted throughout all stages of the thesis. I really admire his extraordinary support throughout my studies as an M.E.Sc student.

Sincere thanks are also given to my good friend Mr. Pritam Das for his great help and contribution during the research work.

I am also thankful to Mr. Djilali Hamza at Queens University for his help and guidance during the experimental work. In addition, I would like to thank all my friends at the Electrical and Computer Engineering Department at the University of Western Ontario and Queens University for the enjoyable experience.

Finally, I would like to thank my parents, M.R.Moussavi and R.Kalantari for their support and encouragement during my studies.

London, Ontario April 2009

Ahmad Mousavi

Contents

List of Figures

NOMENCLATURE

AC	Alternative Current
EMI	Electromagnetic Interference
ESR	Equivalent Series Resistor
DC	Direct Current
LC	Inductor and Capacitor
MOSFET	Metal Oxide Semiconductor Field Effect Transistor
PFC	Power Factor Correction
PWM	Pulse Width Modulation
SSC	Soft-Switching-Cell
UPS	Uninterruptible Power Supply
ZCS	Zero Current Switching
ZVS	Zero Voltage Switching
ZVT	Zero Voltage Transition

Chapter 1

1.1 General Introduction

1.1.1 Power Electronics

It is generally the task of power electronics to convert the electric power available from a power source to the form best suited for the user loads, and some sort of power processor or converter is required to serve as an interface between power source and load. The load may be ac or dc, single-phase or three-phase, and may or may not require transformer isolation from the power source. The power source could be a single-phase or three-phase ac source with line frequency of 50 or 60 Hz; it can be an electric battery, a solar panel or a commercial power supply. This source feeds the input of the power converter, which converts the power to the required form. The converter can be an ac-dc converter, a dc-dc converter, a dc-ac converter or an ac-ac converter.

Power converters typically consist of semiconductor devices such as transistors and diodes, energy storage elements such as inductors and capacitors, and some sort of controller to regulate the output voltage. Transistor type devices like BJTs (Bipolar Junctions Transistors), MOSFETs (Metal Oxide Silicon Field Effect Transistors) and IGBTs (Insulated Gate Bipolar Transistors) are used as switches in power electronic converters and are made to operate as switches that are either fully on or fully off at any given moment in time. These devices can be operated at higher

switching frequencies than thyristor based devices, which helps reduce converter size. While BJTs and MOSFETs are basic devices, IGBTs are hybrid devices that have an insulated gate like a MOSFET but a conduction region that is the same as a BJT.

BJTs were used as switches in SMPS (Switch Mode Power Supplies) in the late 1970's-early 1980's, but since they are current-controlled devices, they are no longer used in SMPS where switches need to be turned on and off at very high frequencies in the kHz range. The MOSFET, being a charge controlled device, is faster than a BJT. When turned on, a MOSFET is equivalent to a resistance between its source and drain ($R_{DS,on}$), while the BJT when fully on is equivalent to a voltage source equal to the saturation voltage between collector and emitter ($V_{CE,sat}$).Thus the conduction losses in MOSFETs are proportional to the square of the on-state current that it is conducting while these losses in a BJT is proportional to the on-state current it is conducting.

The IGBT is a hybrid device that incorporates an insulated gate so that it turns on like a MOSFET and conducts like a BJT in saturation, hence the name IGBT. The IGBT undergoes a MOSFET type turn on, faster than a conventional BJT but its turn off is dependant on the minority carriers present in it during its on state (i.e it undergoes a turn off similar to that of a BJT and has a current tail during its turn off). The IGBT is therefore faster than a conventional BJT but slower than a MOSFET.

MOSFETs are used for lower power applications (typically a few kilowatts) and have lower current and lower voltage ratings (typically a few hundreds of volts) but

higher frequency well in a range of hundreds of kHz while the IGBT is used in higher power applications, they have high voltage and current ratings, but operate at lower frequencies (up to 100kHz).

IGBTs and MOSFETs are widely used in Power Electronic applications such as high frequency inverters used at the front ends of high efficiency ac motor drives, high and very high frequency dc-dc converters, power factor correction modules etc. Diagrams of a N-P-N IGBT and a N-channel MOSFET are shown in Fig.1.1.

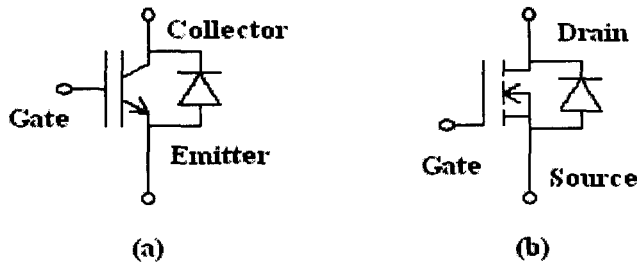

Fig.1.1 (a) Schematic diagram of an IGBT.
(b) Schematic diagram of a power MOSFET.

1.1.2 High Switching Frequency Operation in Power Electronic Converters

The size of the energy storage components of a power electronic converter, such as inductors (L) and capacitors (C), accounts for much of the overall size of the converter. These components are needed to store and transfer energy from the input power supply to the output load in the converter. Their values depend on the frequency that the converter switch is turned on and off. As the switching frequency is increased, the values of the inductors and capacitors decrease and so do their

physical size and weight; therefore the higher the converter switching frequency, the smaller is the converter size.

Higher switching frequency operation, however, results in increased switching losses and Electro Magnetic Interference (EMI) noise emissions, which are described in the next section. Problems associated with switching losses and EMI caused by sudden switching transitions can offset the advantages achieved by operating a converter with a high switching frequency.

1.1.3 Losses in Semiconductor Switches

The semiconductor switches used in power converters are not ideal and are a source of energy losses. The main losses that are associated with these switches are conduction losses and switches losses, which will be described in more detail below.

a) **Conduction losses**

The conduction losses of MOSFETs are due to their behavior as a resistor when fully on - the resistance being equal to $R_{DS,on}$, the on state drain to source resistance. The conduction losses of an IGBT are related to the amount of current flowing in the device and $V_{CE,sat}$, the saturation voltage between collector and emitter.

b) **Switching losses**

In a real semiconductor switch, the switch voltage or switch current do not go to zero instantaneously at the instant of turn-on or turn-off. There is a duration of time during any switching transition (i.e. switch turn-on and turn-off) when there is both

voltage across and current through the switch. The corresponding power loss during each switching instant is the overlapped area of the switch current and voltage waveforms at the instant of turn-on or turn-off of the switch. Since the average power is energy divided by the period, higher switching frequencies lead to higher switching losses. Sharp and sudden switching transitions are also sources of electromagnetic interference (EMI) noise that can affect the performance of a converter and/or other surrounding electrical equipment.

Both the IGBT and MOSFET have anti-parallel body diodes. A MOSFET has a much higher output capacitance between its drain and source than that between collector and emitter of an IGBT. This output capacitance charges up to the off state voltage that the MOSFET is subjected to while the IGBT has a current tailing after it is actually turned off.

In a MOSFET, the main switching losses are caused by the charging and discharging of the output capacitance to and from the off state voltage that the MOSFET is subjected to, while the tailing of current is the primary cause of switching losses in IGBTs. Turning on and turning off the power electronic switches with such switching losses is known as "hard switching". Fig. 1.2 shows the hard switching of power electronic switches in a circuit and the power losses associated with doing so.

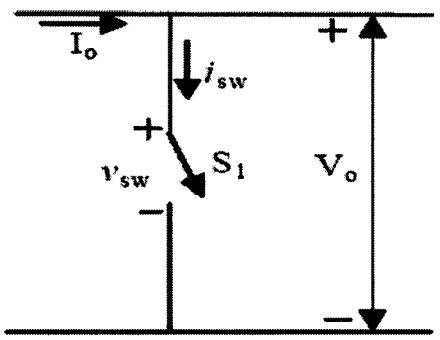

(a)

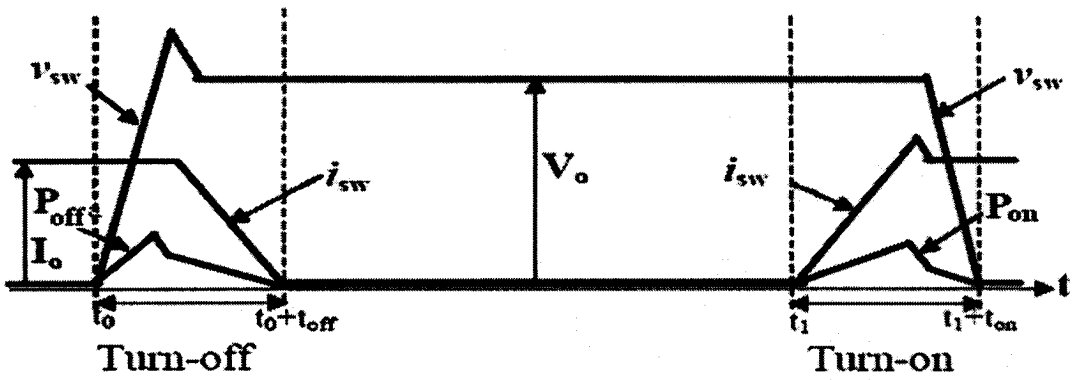

(b)

Fig.1.2 (a) Hard Switching.
(b) Loss of Power during hard switching.

Fig. 1.2(a) shows a power electronic switch S_1 that conducts current i_{sw} when turned on; when turned off the voltage across it is V_o. Fig. 1.2(b) shows the typical current and voltage graphs of the switch S_1 during a whole switching cycle. At t_o, the driving pulse of S_1 is removed so that it gets turned off. S_1 takes time t_{off} to turn off fully. During this time, due to the overlap of the current and voltage waveforms, there occurs a turn off loss represented by the area under the graph P_{off}. At t_1, the driving pulse is applied to the switch S_1 so that it gets turned on. The switch S_1 takes

time t_{on} to get turned on. During this time t_{on}, due to overlap of the current and voltage waveforms of S_1, there occurs a turn-on loss represented in Fig. 1.2(b) by P_{on}.

1.1.4 Diode Reverse-Recovery Current

In addition to semiconductor switches, power electronic converters also contain diodes. A diode is a semiconductor device that allows current to flow in only one direction, from its anode to its cathode, but does not allow current to flow in the negative direction, from its cathode to its anode. An ideal diode will not conduct any negative current, regardless of whatever negative voltage is placed across it, as long as this voltage does not exceed its maximum rated voltage. In reality, however, whenever the current flowing through a diode is decreased to zero, it may momentarily become negative before finally becoming zero, as shown in Fig 1.3.

This negative current is referred to as reverse-recovery current in the power electronics literature since it flows through the device during the time t_{rr} needed by the diode to "recover" from its previous current conduction state. The reverse-recovery current can lead to power losses in the diode and also creates electromagnetic interference (EMI) noise. Fast-recovery diodes with short reverse recovery times (t_{rr}) are therefore widely used in high-frequency converters.

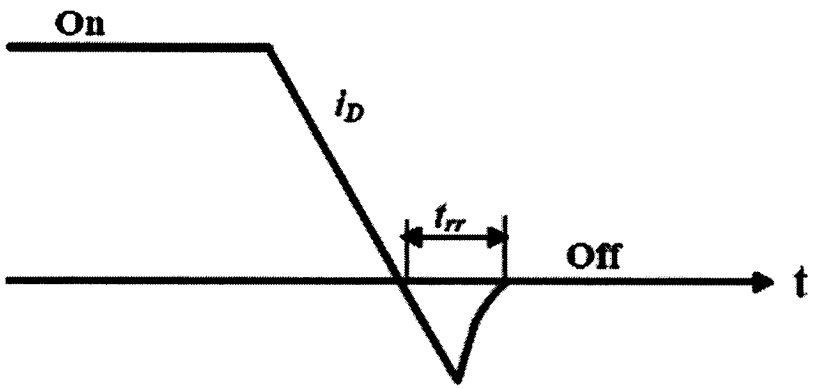

Fig.1.3. Reverse recovery current in a diode.

1.1.5 Soft Switching

The problems of switching losses and EMI associated with hard-switching converter operation can be reduced by using soft-switching. The term "soft-switching" in the power electronics literature refers to various techniques where the switching transitions are made to be more gradual to force either the voltage or current to be zero while the switching transition is being made. EMI is reduced by soft-switching because the switching transitions from on to off and vice versa is gradual and not sudden. Switching losses are reduced since the power dissipated in a switch while a switching transition made is proportional to the overlap of the voltage across the switch and the current flowing through it.

Soft-switching forces either the voltage or the current to be zero during the time of transition; there is therefore no overlap between voltage and current and therefore (ideally) no switching loss. There are, therefore, two types of soft-switching: zero-

voltage switching (ZVS) and zero-current switching (ZCS). Although there are many ZVS and ZCS techniques, there are general principles associated with each type.

For power converters operating with high switching frequencies, the MOSFET is the semiconductor device that is most commonly used. The circuit symbol for a MOSFET is shown in Fig.1.4, along with an anti-parallel diode (which is the body diode that is internal to the device) and a capacitor C_{ds} that is across the device's drain and source. C_{ds} usually consists of an internal capacitance associated with the device and an additional external capacitor. The MOSFET can turn on with ZVS if it is somehow ensured that current is flowing through the body diode to clamp the drain-source voltage to zero just before turn-on. The MOSFET can turn off with ZVS because C_{ds} prevents the voltage from rising abruptly as the device is turned off.

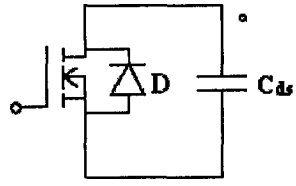

Fig.1.4 ZVS MOSFET implementation

A MOSFET can be made to operate with ZCS if an inductor is added in series to it as shown in Fig. 1.5. The MOSFET can turn on with ZCS because the inductor limits the rise in current so that the current flowing through the MOSFET is almost zero as the device is being turned on. The MOSFET can turn off with ZCS if a negative voltage is somehow impressed across the inductor-MOSFET combination so that current falls to zero at a gradual rate due to the inductor.

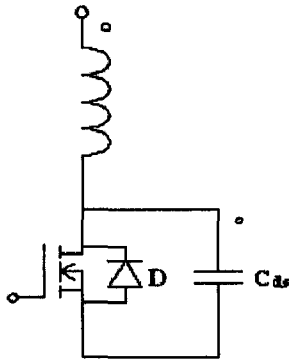

Fig.1.5 ZCS IGBT implementation.

Although both ZVS and ZCS operations can reduce the switching losses of a MOSFET, ZVS is preferred because ZVS can substantially reduce the losses caused by the discharging of C_{ds} into the device when it is turned on whereas ZCS cannot.

It should be noted that although soft-switching can reduce switching losses, conduction losses that exist when current flows through a MOSFET/IGBT/ Diode will still exist.

1.2 DC-DC Converters

Dc-dc converters convert an available unregulated dc input voltage into a regulated dc output voltage of a different magnitude and/or polarity as required by a particular load. Most dc-dc converters are switch-mode converters that operate with active semiconductor devices like MOSFETs and IGBTs, acting as on-off switches. These switches are required to undergo repetitive and periodic turn on and turn off. The output dc voltage in such converters are dependant on the duty cycle D (<1)

which is defined as the length of time that the switch is on (t_{on}) over the duration of the switching cycle ($T_{sw}=1/f_{sw}$).

$$D = t_{on}/T_S \tag{1-1}$$

The two most basic types of dc-dc converters are the buck converter (Output voltage is a stepped down value of the input voltage) and boost converter (Output voltage is a stepped up value of the input voltage). Other types of dc-dc converters are buck-boost, Cuk, Sepic and Zeta etc. The circuit diagram of a boost converter is shown in Fig.1.6 along with the typical voltage and current waveforms in Fig1.7.

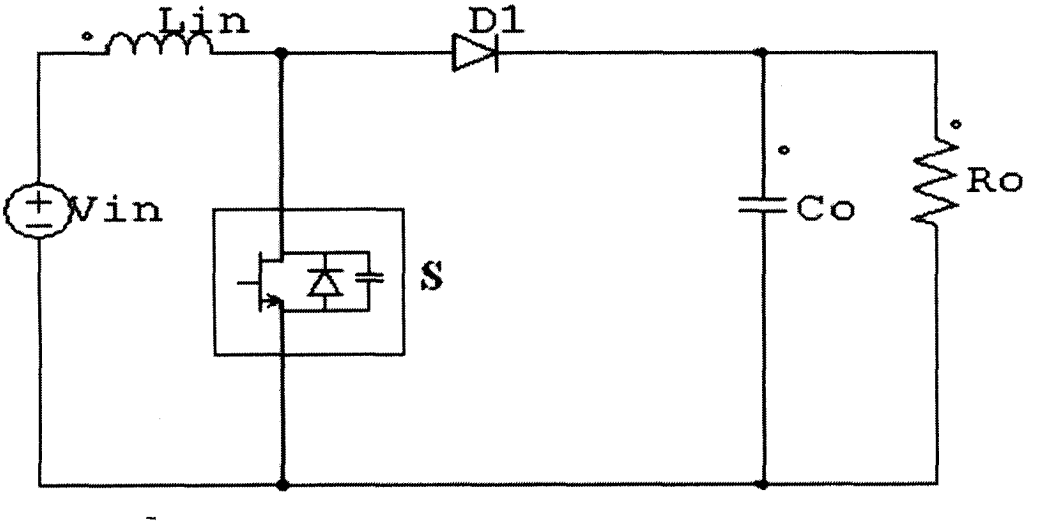

Fig.1.6 A dc-dc boost converter

The converter shown has a MOSFET as the power electronic switch since it is best suited for high switching frequency converters. In steady state, after the switches are turned on, the whole input voltage is applied across the input inductor L_{in} and it stores up energy. When the switches are turned off, a negative voltage equal to ($V_{in} - V_o$) is applied across the inductor and the energy stored in the inductor is delivered to

the output capacitance C_o. The steady state output voltage of the boost inductor must always be greater than the input voltage as the ratio of the output to input voltage is:

$$\frac{V_o}{V_{in}} = \frac{1}{1-D} \tag{1-2}$$

In order to operate the MOSFET switches in the boost converter, a periodic pulse (V_{ge}) such as shown in Fig.1.7(b) must be applied between the gate(g) and the emitter(E) of the device through a drive circuit. The MOSFET is on when the pulse V_{ge} is high and off when it is low. Since $T_{on} = DT_{sw}$, the duty cycle of the converter and hence the ratio of the output to input voltage, is determined by the width of the pulse V_{ge} so that it is the pulse width that is ultimately used to control and regulate the output voltage. This method of controlling the converter output, which is frequently used, is known as pulse width modulation control or PWM control.

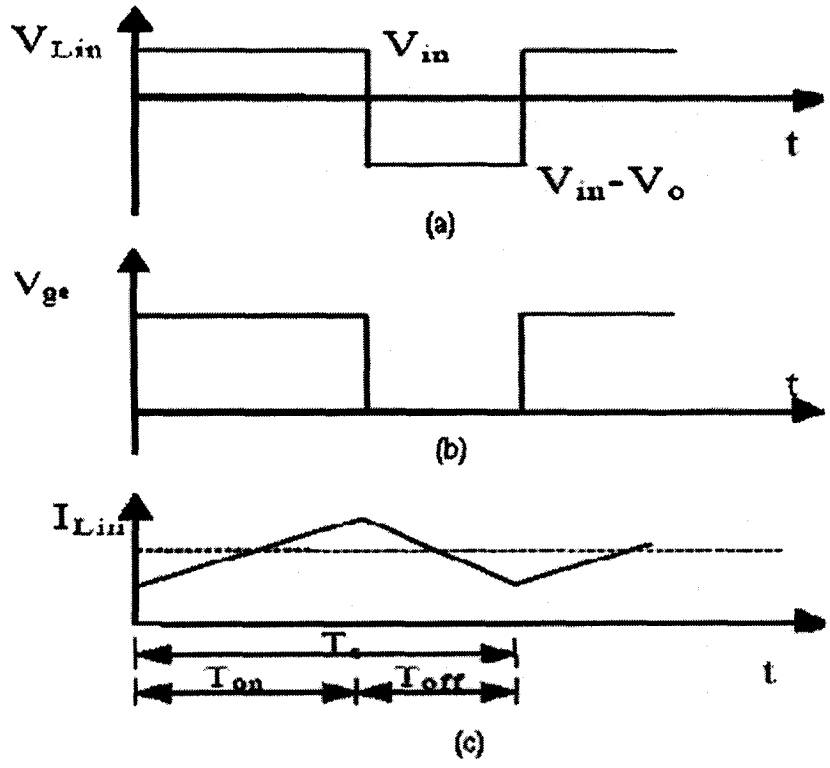

Fig.1.7 a)Waveform of the voltage across input inductance L_{in} of a boost converter.
b)Waveform of the voltage at the gate of the switch in a boost converter.
c) Waveform of current through the input inductance in a boost converter.

1.3 Full-Bridge Boost Converters

Full-bridge boost converters like the one shown in Fig.1.8 are very attractive for applications where an output dc voltage that is considerably larger than the input voltage is needed. Such applications include fuel cell power conversion, medical power supplies, and power supplies for electrostatic applications. These converters are essentially boost converters that contain a step-up transformer so that they can do additional voltage "boosting" without the very large duty ratios (D) needed with the boost converter shown in Fig.1.8.

The converter operates like a boost converter as the current in inductor Lin is increased whenever switches from the same leg are on and it is decreased whenever a pair of diagonally opposed switches is on as energy is transferred to the output through the transformer and the output diodes. It should be noted that there must always be a path for the input inductor current to flow through the full bridge switches at all times.

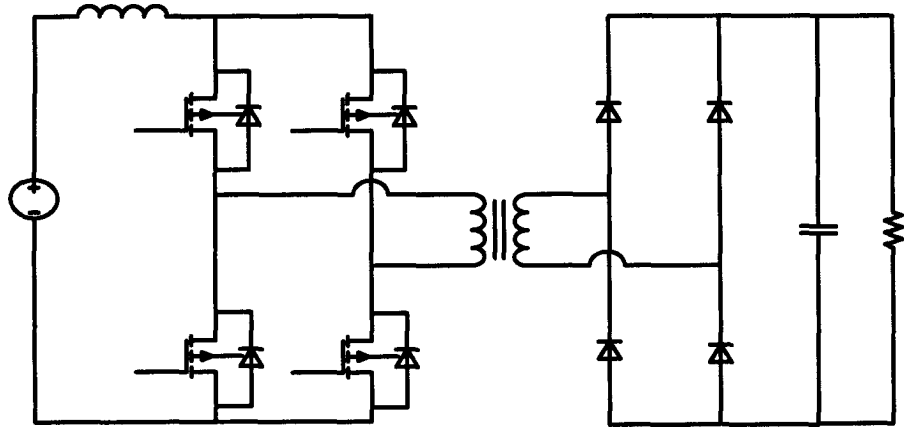

Fig.1.8 Current-fed PWM full-bridge boost converter

A full-bridge boost converter can be implemented with either zero-voltage switching (ZVS) or zero-current switching (ZCS) depending on the application. ZVS is implemented in applications where the input voltage is high, the input current is low or medium, and switch turn-on switching losses are dominant. ZCS is implemented in applications where the input current is high (regardless of what the input voltage is) and conduction losses are dominant. The focus of the thesis will be on ZCS full-bridge boost converters.

1.4 Literature Review

The first ZCS full-bridge converters that were proposed were resonant converters [11], [17], [18]. ZCS resonant converters use an inductive – capacitive (L-C) circuit to create oscillatory (usually sinusoidal) switch current waveforms so that ZCS turn-on and turn-off conditions can be achieved for the power switches. The converter shown in Fig. 1.9 is the conventional full-bridge boost converter with added L and C component to create the resonant circuit.

Most resonant converters, however, suffer from high peak switch voltage or current stresses in comparison to conventional PWM converters. This leads to higher conduction losses and higher voltage and current ratings for the power switches and other circuit components. Another disadvantage is that most resonant converters operate with variable switching frequency control (the output voltage is controlled by varying the converter switching frequency). If operation over a wide range in input voltage and output load is required, most resonant converters must operate with a wide switching frequency range. This makes it difficult to optimize the design of the converter and its control.

In the circuit proposed in [11] the converter is a fixed frequency resonant ZCS current fed converter (Fig.1.9) or a variable frequency resonant converter in [17]-[18] that generates a considerable amount of circulating current in the full bridge so that the switches can turn off with ZCS. Examples of variable frequency resonant converters are shown in Fig.1.10 (a),(b). It should be noted that the circulating

current is not transferred to the load and does little but add to the conduction losses of the converter. Although the converter is more efficient than it would be if ZCS was not implemented, the gains in efficiency are not as much as what they could be due to these losses.

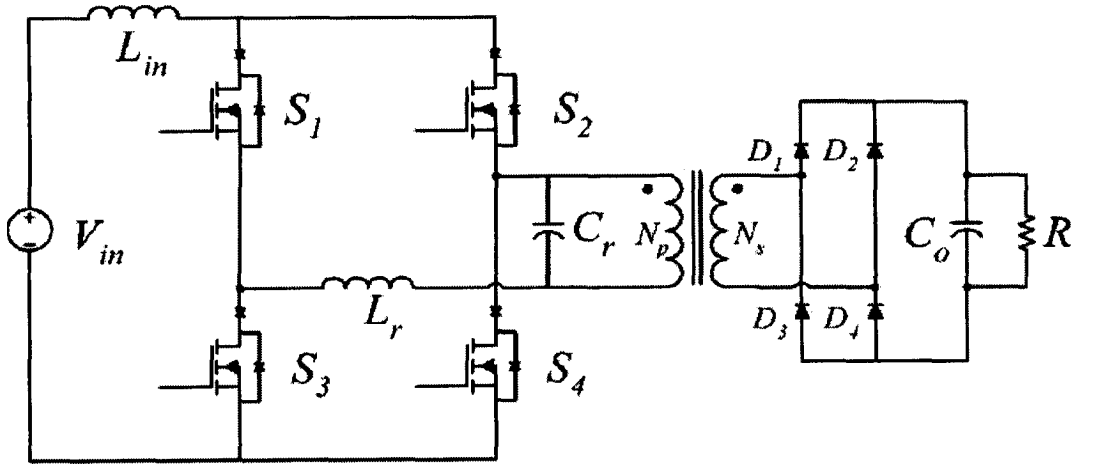

Fig.1.9 Fixed frequency resonant ZCS current fed converter proposed in [11]

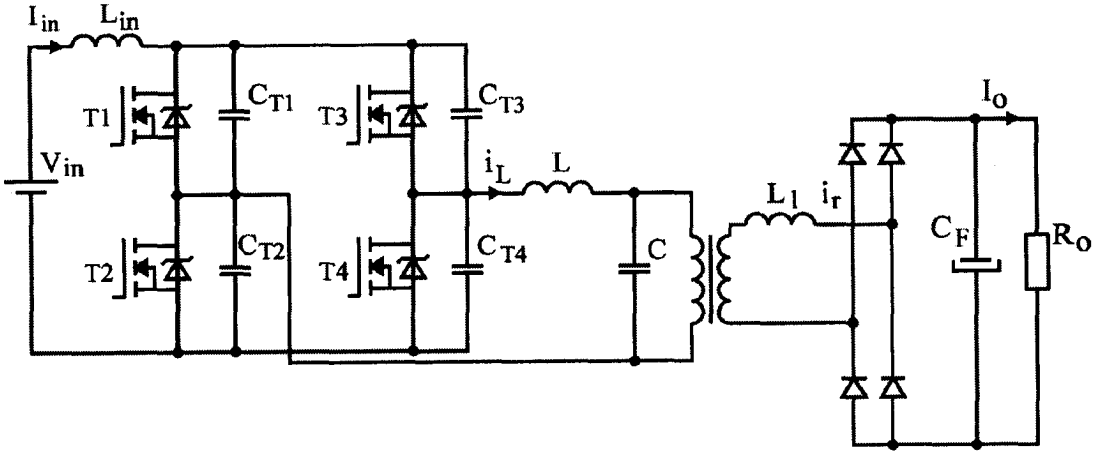

Fig.1.10 (a)

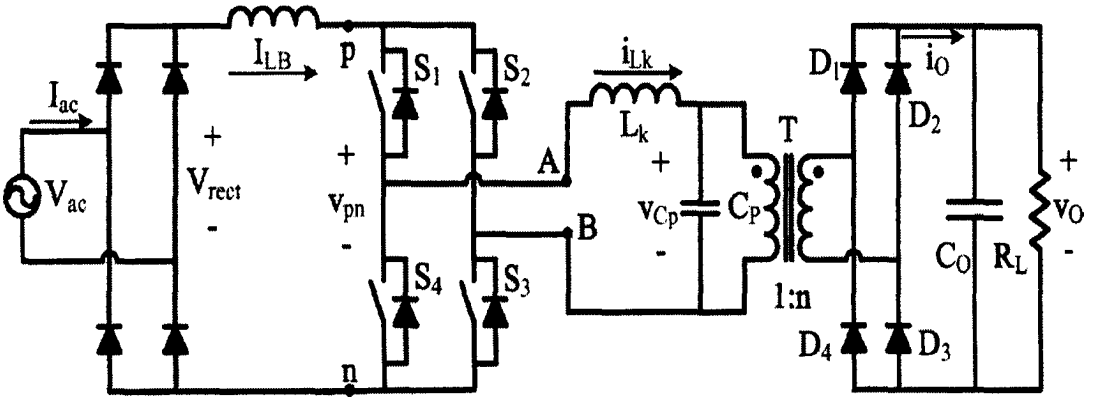

Fig.1.10 (b)

Fig.1.10 (a), (b) Variable frequency resonant ZCS current fed converter

Most recent soft-switched full-bridge boost converters can be classified as being resonant-transition converters, and have the advantages of conventional PWM converters and resonant converters. They use an additional or auxiliary circuitry that is not a part of the main power circuit to help the main converter switch turn on and off with ZCS. This auxiliary circuit typically consists of an active power switch and passive elements such as diodes, inductors, and capacitors. The operation of the auxiliary circuit only occurs during the turn-on and turn-off of the main converter switch and only a very small portion of switching cycle.

To realize ZCS for the main switch, the basic idea behind this type of auxiliary circuit is to activate the circuit by turning on an auxiliary switch placed properly in the circuit for a small fraction of the switching cycle and just before the semiconductor switch has to be turned off. By activating the circuit, a capacitor placed in the circuit is forced to undergo resonance with some inductance properly

placed with the switch so that the capacitor, under resonance, creates a counter voltage across the inductor-switch pair thus forces the current in the switch to be reduced to zero before the pulse at the gate of the switch is removed. Eventually the switch will be turned off with zero current.

Since the auxiliary circuit is active for only a small portion of the switching cycle, the circuit behaves almost exactly like a conventional PWM converter, but with smoother voltage and current waveforms especially during switching transitions. The components in the auxiliary circuit handle a fraction of the power than the main power circuit components must handle, thus allowing small components to be used. This is especially true of the auxiliary switch, which can be a device with ratings smaller than that of the main power switch and therefore operate with fewer switching losses, so that whatever new switching losses that are created by the auxiliary switch are more than offset by the reduction of switching losses in the main switch. Numerous auxiliary circuits for ZCS-PWM full-bridge converters have been proposed in the power electronics literature [12]-[16].

One of the basic and early versions of such a circuit is shown in Fig.1.11. The auxiliary circuit is simple as it incorporates only one extra inductor and a capacitor and one auxiliary switch, but its drawback is the high current peak in main switches. This high current peak in the main switches calls for the need of switches with higher current ratings, and such switch tends to have higher conduction losses. Also high current peaks tend to create additional unwanted conduction losses. Moreover, due to the resonant capacitor charging to as high as twice the output voltage during the

operation of the auxiliary circuit, there is a need for a resonant capacitor with bigger size since a capacitor's physical size is dependant on its voltage ratings.

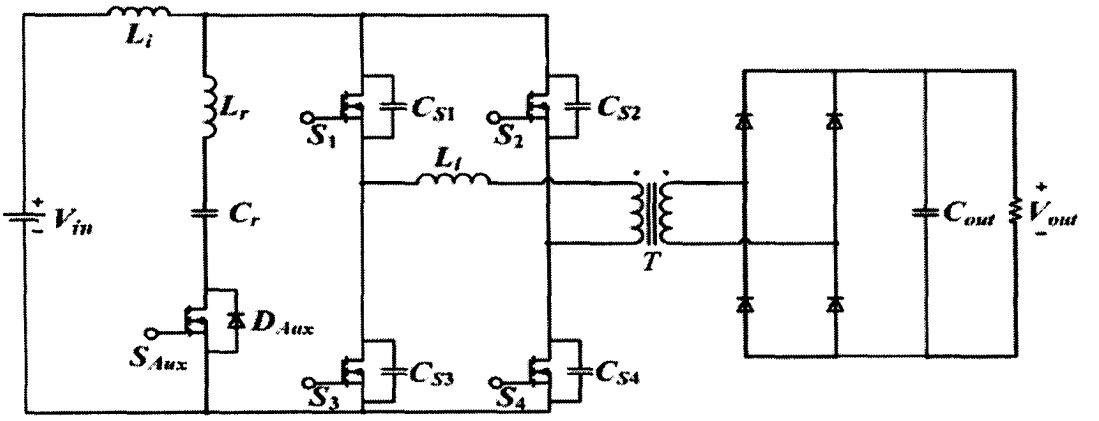

Fig.1.11 ZCS full-bridge PWM boost converter

In some cases the converter uses an active auxiliary circuit that is connected in parallel to the full-bridge and used to divert current away from the switches in the bridge before they are to be turned off to realize ZCS turn off of devices [13]-[18]. This circuit is activated just before any switches are to be turned off and is deactivated shortly afterwards. Since the circuit is active for only a short length of time, there is less circulating current compared to the fixed frequency resonant converters, but this current is still significant. All the energy from this current is trapped in the primary side of the converter and it contributes to losses. Examples of such converters were proposed in [15] and [16] and are shown in Fig.1.12 (a), (b) respectively. Both converters have an auxiliary circuit connected to the full-bridge in parallel.

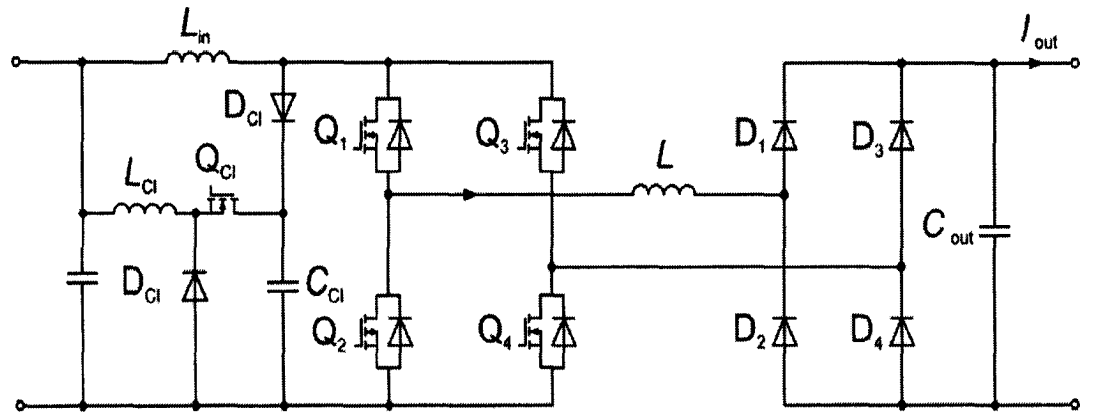

(a)

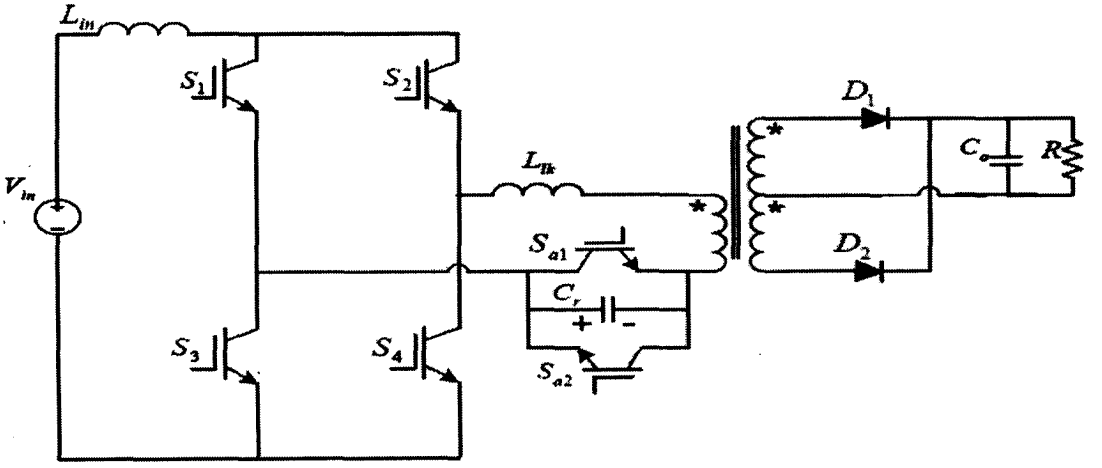

(b)

Fig.1.12 Current-fed converters with parallel auxiliary circuit (a) [16] (b) [15]

The additional circulating current also contributes to increased peak current stresses in the full-bridge switches as these switches must conduct the current that they are supposed to conduct, to feed the load and the circulating current. Devices that can withstand higher peak current stresses than those found in conventional boost full-bridge converters are needed as the converter switches [13]-[16].

Fig.1.13 shows the circuit proposed in [13]. In the paper, high rated switches have been used for the experimental results, so the switches can stand the current peak that occurs because of the additional circulating current.

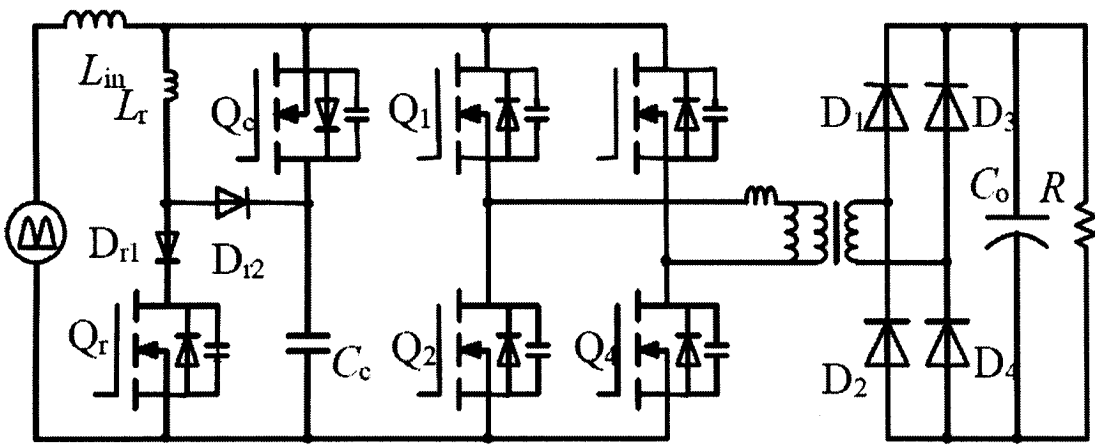

Fig.1.13. Current fed full-bridge converter proposed in [13]

In some other proposed converters, diodes are placed in series with the switches so that current does not flow through the body-diodes of the switches and circulating current is reduced [14]. The circuit proposed in [14] is shown in Fig.1.14. Although conduction losses are increased, they may be smaller than what they would be if the diodes were not added, but this is at the cost of the additional diodes. Some converters avoid using diodes by using reverse blocking IGBTs [12], but they are more expensive than regular IGBTs and not appropriate for low voltage input applications.

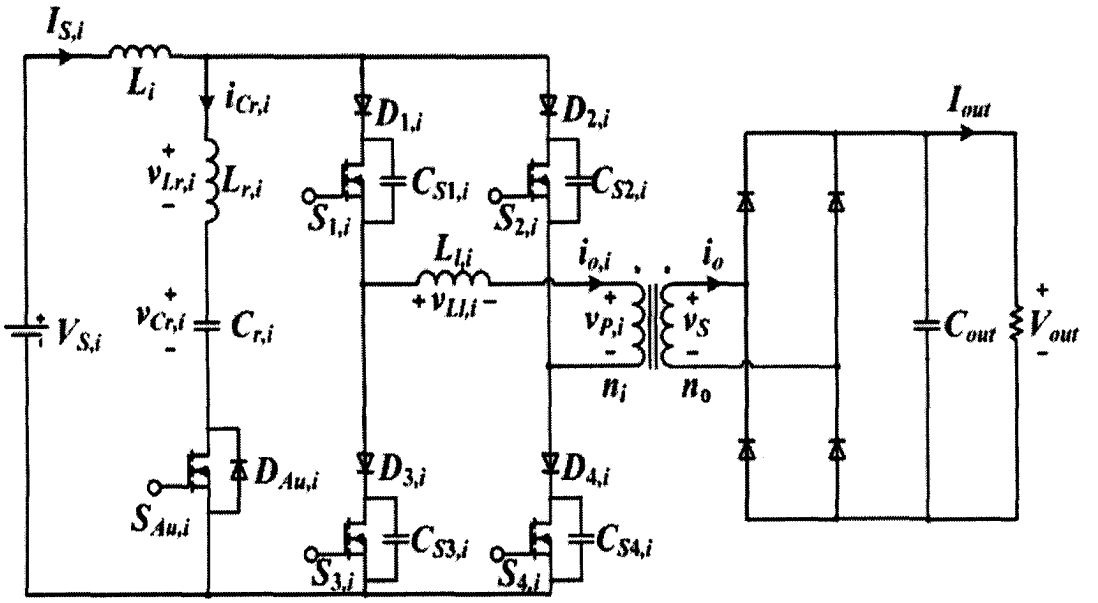

Fig.1.14. Full-bridge boost converter with current-blocking diodes proposed in [14]

Other drawbacks that can be found in previously proposed ZCS full-bridge boost converters include the need for a high side driver [15] for the auxiliary circuit switch(es), which makes the driving of this switch(es) more complicated and the appearance of voltage spikes and/or the significant voltage ringing that can appear across the main converter switches [11]-[18]. The later is due to the output capacitances of the switches resonating with the leakage inductance of the main transformer during their turn off. The spikes and ringing will appear across the secondary diodes as well. This creates a need for higher voltage rated devices, which will increase the cost and the losses in the converter.

1.5 Thesis Outline

This thesis is organized as follows:

In Chapter 2, a new auxiliary circuit that allows the main power switches in ZCS-PWM full-bridge dc-dc boost converters to operate with soft-switching is proposed and its operation is described.

In Chapter 3, the circuit analysis of a ZCS-PWM full-bridge dc-dc boost converter operating with the proposed auxiliary circuit is presented for the various modes of operation that the converter goes through during a switching cycle, as described in Chapter 2. Important mathematical equations describing voltages and currents of different circuit components during the modes of operation are derived.

In Chapter 4, the conditions that ensure the soft switching of the main switches in the converter are derived with the help of the mathematical equations derived in Chapter 3. Also, characteristics curves showing the behavior of the converter with respect to the variation of different passive components are presented. An experimental prototype is designed using these characteristic curves. Converter component values are chosen using a design procedure that will be presented and demonstrated with an example.

In Chapter 5, experimental voltage and current waveforms for the prototype designed in Chapter 4 are presented to validate the concept of the proposed auxiliary circuit. Efficiency graphs for a full-bridge boost converter with and without the proposed auxiliary circuit are presented to demonstrate the effectiveness of the circuit in increasing converter efficiency.

In Chapter 6, the contributions and conclusions of this thesis are presented and suggestions for future work are given.

Chapter 2

A New ZCS-PWM Full-Bridge Boost Converter

2.1 Introduction

It was seen in Chapter 1 that previously proposed auxiliary circuits applied to ZCS-PWM full bridge converters introduce additional current and voltage stresses on the converter devices. These stresses can cause additional conduction losses in the devices that can reduce the savings of energy realized by the soft-switching of the main switches. For example, the circulating energy that exists when the auxiliary circuit of some ZCS-PWM converters is operating is trapped in the circuit and creates additional losses.

With these issues in consideration, the auxiliary circuit shown in Fig. 2.1 is proposed. The circuit consists of auxiliary diode D_{aux}, inductor L_{r2}, energy feed-forward transformer T_{aux}, auxiliary switch Q_{aux}, diodes D_{S1} and D_{S2} placed at the secondary and the tertiary windings of the transformer T_{aux} and inductor L_{r1} placed in series with the main switches Q_{1-4} (shown in Fig.2.2).

The main concept behind this auxiliary circuit is to add a transformer to create a counter voltage in the circuit to reduce the peak value of the resonating capacitor voltage (V_{Cr}), which is the main cause of the increased peak current in the auxiliary switch. Clamping the primary of the energy feed-forward transformer with a suitable stepped down value of the output voltage imposes this counter voltage. Adding the transformer also creates a path to take out the circulating energy in the auxiliary

circuit and transfer to the output, thus increasing the overall efficiency of the converter. This energy feed-forward is accomplished by suitably connected diodes at the transformer secondary and tertiary windings.

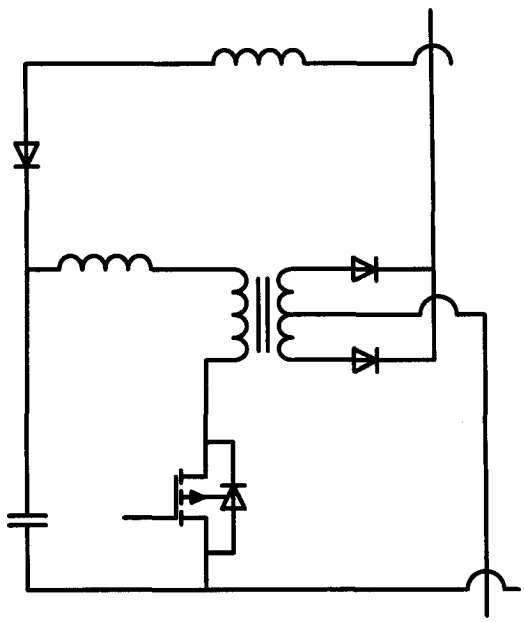

Fig.2.1. The auxiliary circuit used in the proposed converter

The placement of the proposed auxiliary circuit in a ZCS-PWM dc-dc full-bridge boost converter is proposed in this section and shown in Fig. 2.2. The proposed converter is well-suited in low input voltage / high output voltage PWM dc-dc full-bridge boost converters. This auxiliary circuit is the most efficient when compared to several others implemented in a conventional PWM boost converter. Most other auxiliary circuits (i.e. [19]-[24]), however, cannot be adapted for use in ZCS-PWM isolated boost converters (i.e. fuel cell converters) due to their circuit structure or the

fact that they create unwanted current and voltage stresses on the main devices and undergo high circulating current losses

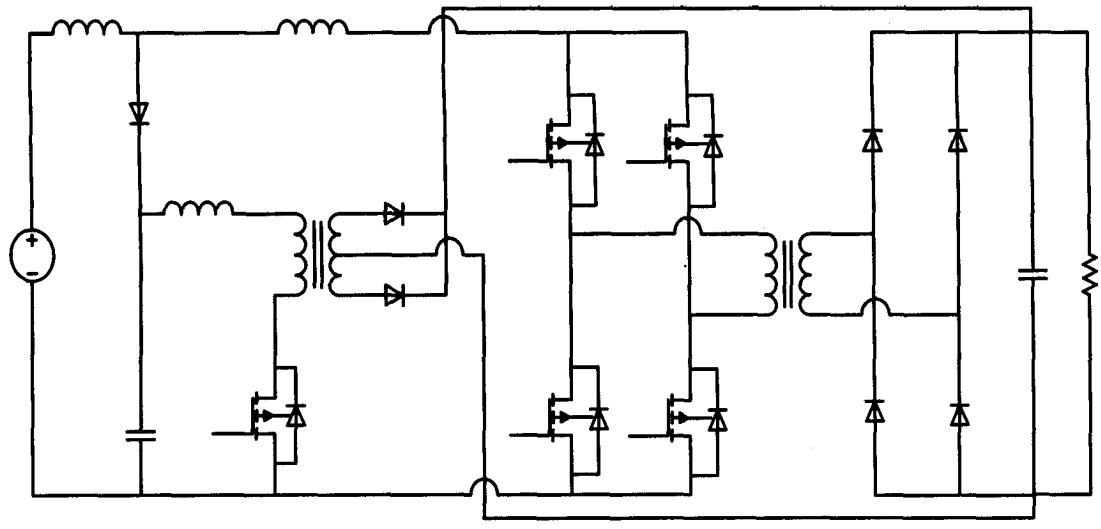

Fig. 2.2. Proposed ZCS full-bridge boost converter

2.2 Converter Operation

In this section, the steady state operation of the proposed full-bridge boost converter will be explained in terms of the different modes or phases that the converter undergoes over a steady-state switching cycle. These modes are distinct from each other in terms of flow of current and voltage across different circuit components. By steady state operation of the converter, it is implied that, at the beginning of each switching cycle, the components of the converter are at the same state with respect to their voltages and currents as they were in the previous

switching cycle, or in other words, the voltage and current waveforms of all components of the converter are identical for every switching cycle in steady state.

The voltage and current waveforms of the different components of the converter during each mode over a switching cycle in steady state will be shown to illustrate the operation of the converter. These modes of operation are important for deriving mathematical equations through circuit analysis that will describe the steady state operation of the converter mathematically. These mathematical equations will be needed to derive the characteristics of the converter with respect to different circuit components and help in designing a prototype.

The following assumptions are made regarding different circuit components while analyzing the proposed boost converter topology:

1) Input boost inductor L_{r1} is large enough to be considered as a constant current source.
2) Output capacitor C_o is large enough to be considered as a voltage source equal to the desired output voltage.
3) All semiconductor switches are ideal *i.e,* they have zero voltage drop across them while they are on and they have no output capacitance across them.
4) The recovery time of each diode is zero.
5) The energy feed-forward transformer is ideal *i.e* it has infinite magnetizing inductance, zero leakage inductance and no lossy components associated with it.

The boost converter with the proposed auxiliary circuit undergoes nine different modes of operation over one switching cycle at steady state. In the following section, different modes of operation of the boost converter along with the proposed auxiliary circuit are described:

Mode 0 ($t < t_0$) (Fig.2.4(a)): Input current I_{in} flows through switches Q_3 and Q_2, and energy is transferred to the load through diodes D_2 and D_3.

Mode 1 ($t_0 < t < t_1$) (Fig.2.4(b)): At time $t = t_0$, both Q_1 and Q_4 are turned on. Due to the primary transformer leakage inductance, the transfer of current to these switches is gradual so that they turn on with ZCS, and some energy continues to be transferred to the output. Eventually, no current flows in the transformer primary except the magnetizing current (which is neglected here), and the dc bus is shorted with half of I_{in} flowing through one full-bridge leg and the other half flowing though the other leg. Since the current splits between two legs of the bridge, losses will be half the case where only one leg is shorted.

Mode 2 ($t_1 < t < t_2$) (Fig.2.4(c)): At $t = t_1$, the auxiliary switch Q_{aux} is turned on and C_r begins to resonate with L_{r2} and discharge. The auxiliary transformer primary voltage is clamped to $V_x = V_o \frac{N_1}{N_2}$ from time t_2 to t_4 and the secondary diode D_{s1} is forward biased. Circulating energy from the auxiliary circuit is transferred to the

output during this time through T_{aux} and D_{s1}. This mode ends when the voltage of Cr (V_{Cr}), reaches zero and diode D_{aux} turns on.

Mode 3 ($t_2 < t < t_3$) (Fig.2.4(d)): At $t = t_2$, the voltage across C_r reaches zero and D_{aux} starts to conduct as C_r continues to resonate with L_{r2} and the voltage across it becomes negative. This negative voltage appears across the dc bus and thus current begins to be diverted away from the full-bridge switches.

Mode 4 ($t_3 < t < t_4$) (Fig.2.4(e)): At $t = t_3$, the current through the main switches becomes zero and begins reversing direction by flowing through the body diodes of the switches. Switches Q_2 and Q_3 can be turned off softly at any time while current is flowing in their body diodes. Current in the auxiliary circuit is positive but decreasing.

Mode 5 ($t_4 < t < t_5$) (Fig.2.4(f)): At $t = t_4$, the body diode of Q_{aux} starts conducting and the switch can be turned off softly after this instant. During this mode, all the body diodes of all converter switches conduct current and the current coming out of the bridge flows through L_{r1} and D_{aux} while charging C_r. Energy is transferred from the auxiliary circuit to the load through T_{aux} and D_{s2}.

Mode 6 ($t_5 < t < t_6$) (Fig.2.4(g)): At $t = t_5$, the current in the body diode of Q_{aux} goes to zero. During this mode, the voltage across C_r increases in resonance with L_{r1} while

the current flows through the body diodes of the full-bridge switches. At the end of this mode the voltage across C_r reaches $V_{pri} = V_o/N$.

Mode 7 ($t_6 < t < t_7$) (Fig.2.4(h)): At $t = t_6$, the current in the body diodes of the full-bridge switch becomes zero, and some input current starts to flow through L_{r1}, Q_1 and Q_4. The remaining input current continues to charge C_r and the voltage across it rises. Energy begins to be transferred to the load through D_1 and D_4. At the end of this mode the voltage across C_r charges up to V_{Cr0}.

Mode 8 ($t_7 < t < t_8$) (Fig.2.4(i)): At $t = t_7$, all the input current flows through the bridge and none through C_r. The converter is in an energy transfer mode.

The proposed ZCS-PWM full-bridge boost converter has the following features:

(i) The presence of a transformer in the auxiliary circuit provides a path for energy that would otherwise be trapped in the auxiliary circuit. Energy can be transferred to the output instead of contributing to conduction losses.

(ii) The auxiliary circuit is adaptive as greater the energy that would otherwise be trapped in the circuit, greater the energy that is transferred to the output, since trapped auxiliary circuit energy is a cause of circulating current. This means that the converter can be made to operate with little additional circulating current regardless of whether it is operating with a light load or a heavy load. This property does not exist in most other ZCS-PWM full-bridge boost converters as

they have a considerable amount of circulating current when operating under light load conditions.

(iii) Since the proposed converter has little additional circulating current regardless of load, it does not need additional diodes connected in series with the full bridge switches to prevent current flowing through their body diodes. There are therefore no conduction losses due to series blocking diodes unlike several other ZCS-PWM full-bridge boost converters.

(iv) The peak current stress of the switches is the same as that of a switch in a conventional PWM boost full-bridge converter, as D_{aux} blocks any auxiliary circuit current from flowing into the full-bridge.

(v) One of the drawbacks of a conventional current-fed full bridge converter is that it lacks a DC bus capacitor across the full bridge section so that there can be uncontrolled voltage spikes during turn off of the bridge devices owing to resonance between their output capacitance and leakage inductance which can damage the bridge devices. It can be seen from Fig. 2.3 that the full bridge switches do have an additional voltage stress in the form of a controlled voltage hump and not a voltage spike. The rise of this voltage hump is restricted by the size of C_r, L_{r1} and L_{lk}. This allows lower rated devices to be used as the full bridge switches.

Voltage and current waveforms of different converter components are shown in Fig. 2.3 and the flow of currents in the circuit during a whole switching cycle is shown in Fig. 2.4(a) to Fig. 2.4(i).

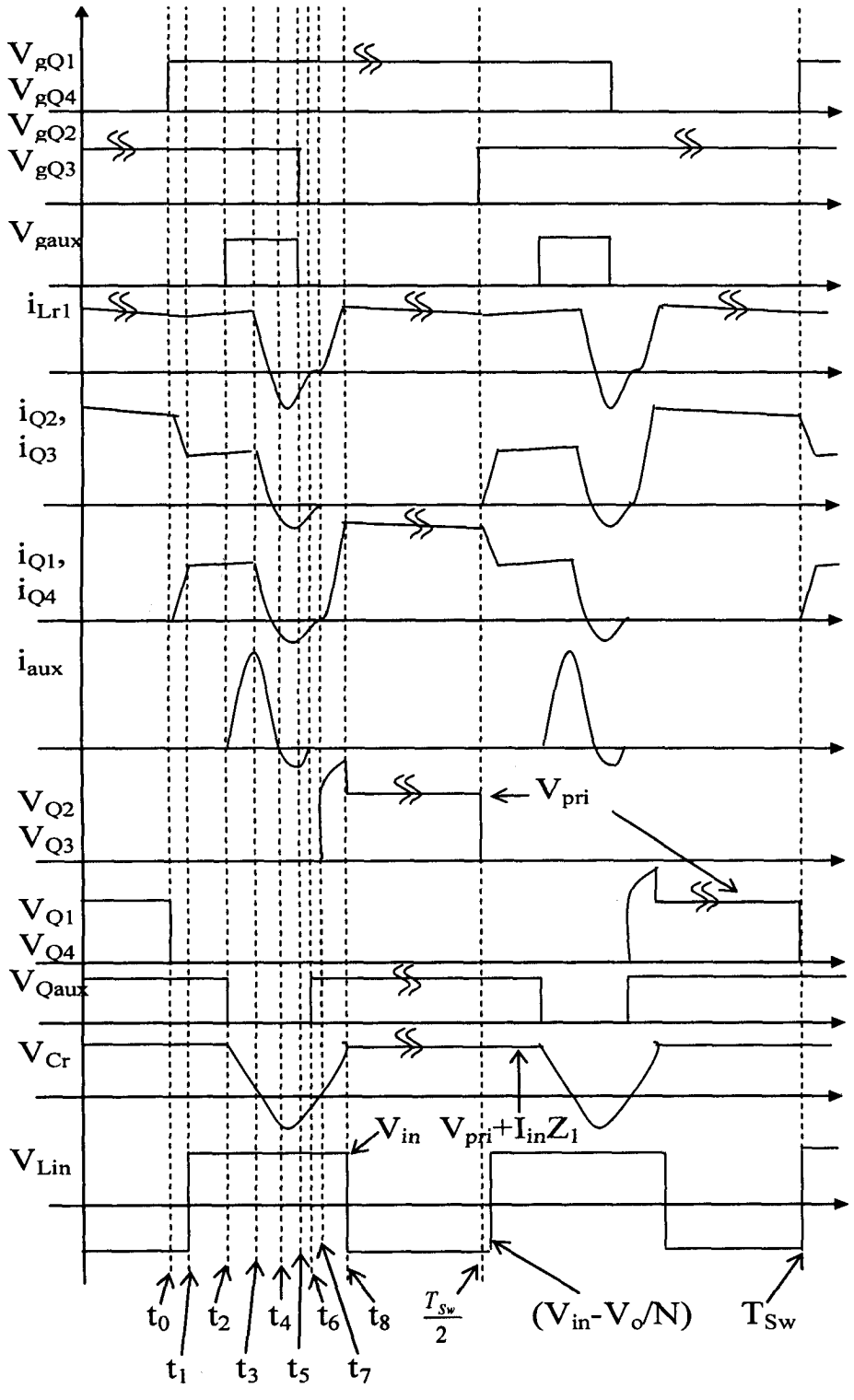

Fig.2.3 Voltage and current waveforms for different circuit components of a boost converter with proposed auxiliary circuit operating in steady state.

Circuit diagrams showing current flow in different modes of operation:

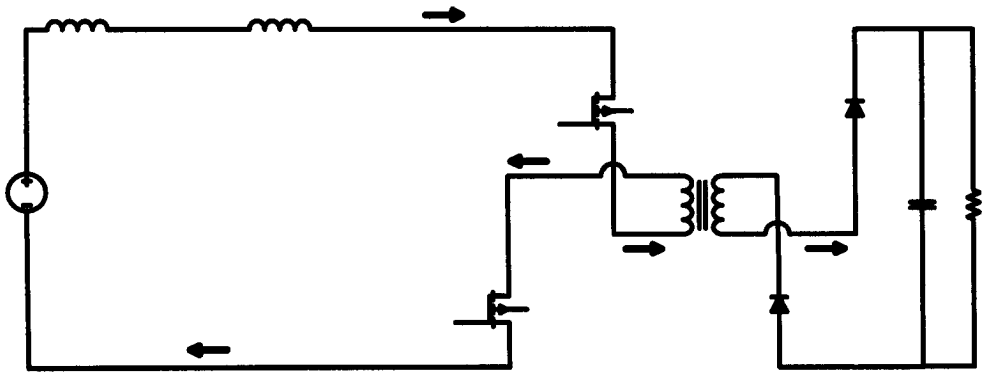

Fig. 2.4(a) Current flow in Mode 0

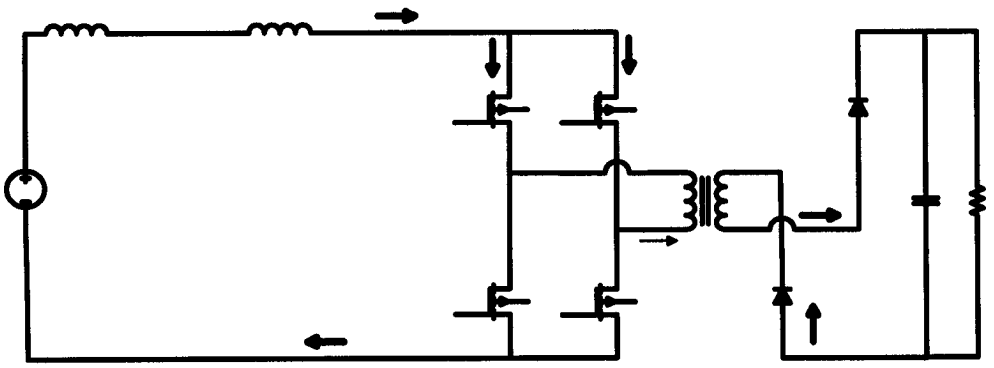

Fig. 2.4(b) Current flow in Mode 1

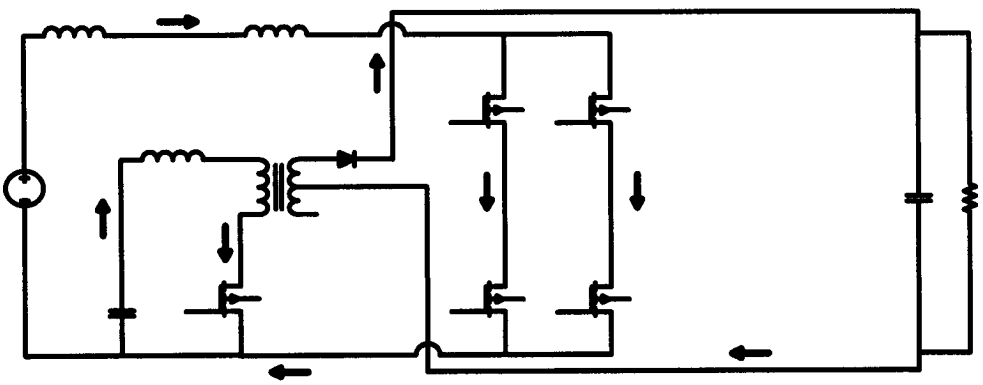

Fig. 2.4(c) Current flow in Mode 2

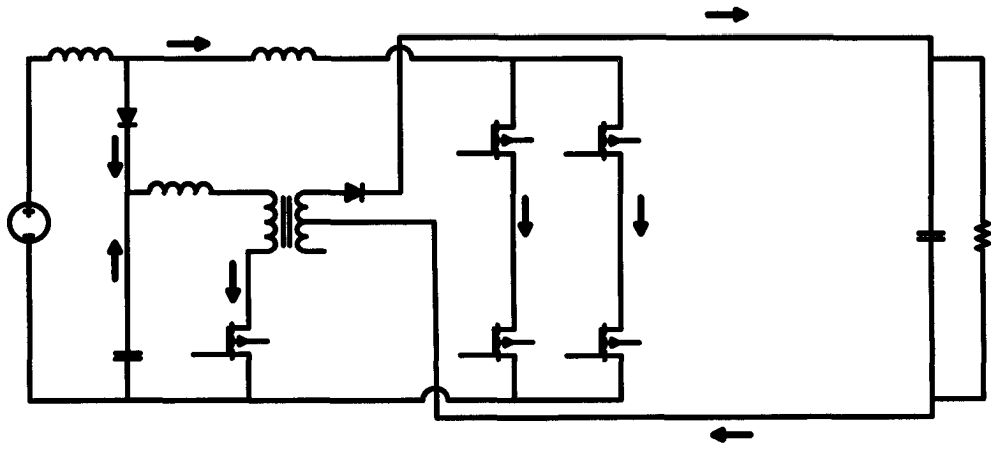

Fig. 2.4(d) Current flow in Mode 3

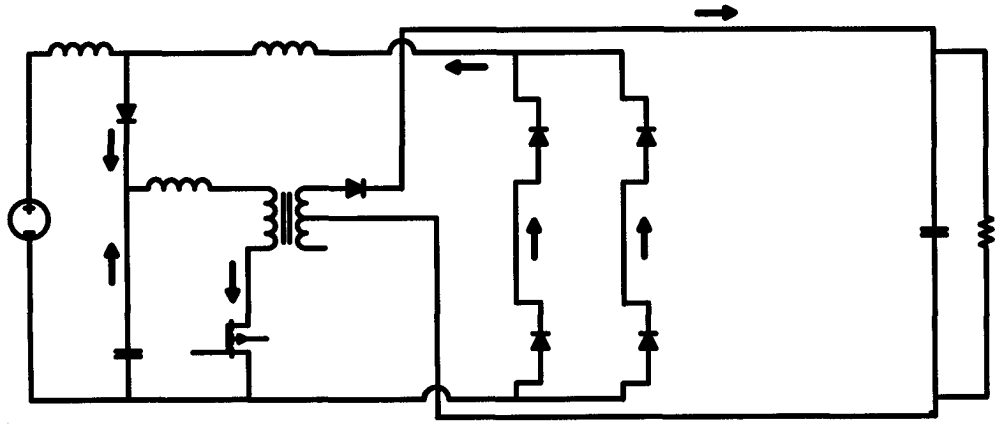

Fig. 2.4(e) Current flow in Mode 4

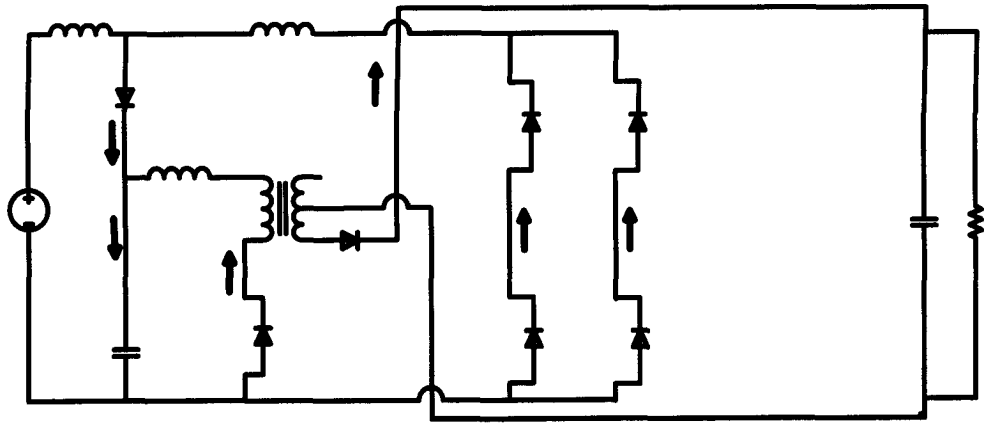

Fig. 2.4(f) Current flow in Mode 5

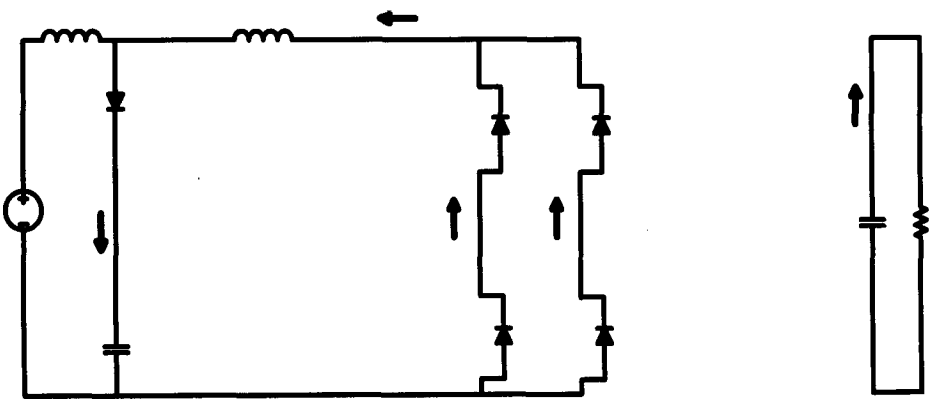

Fig. 2.4(g) Current flow in Mode 6

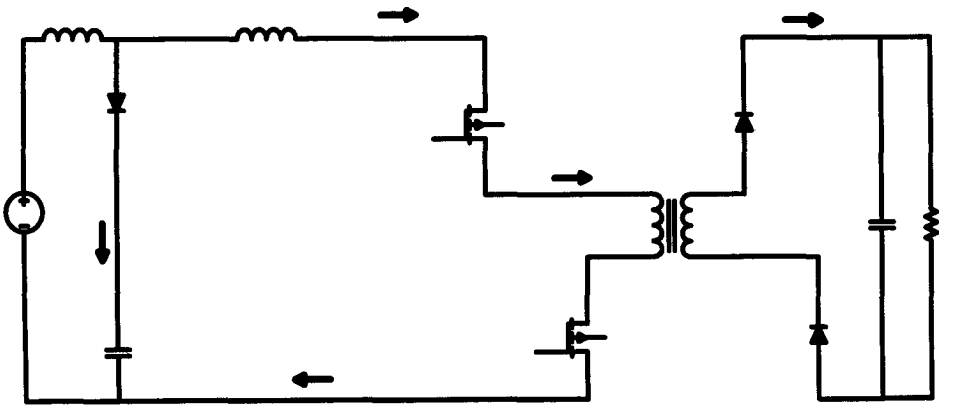

Fig. 2.4(h) Current flow in Mode 7

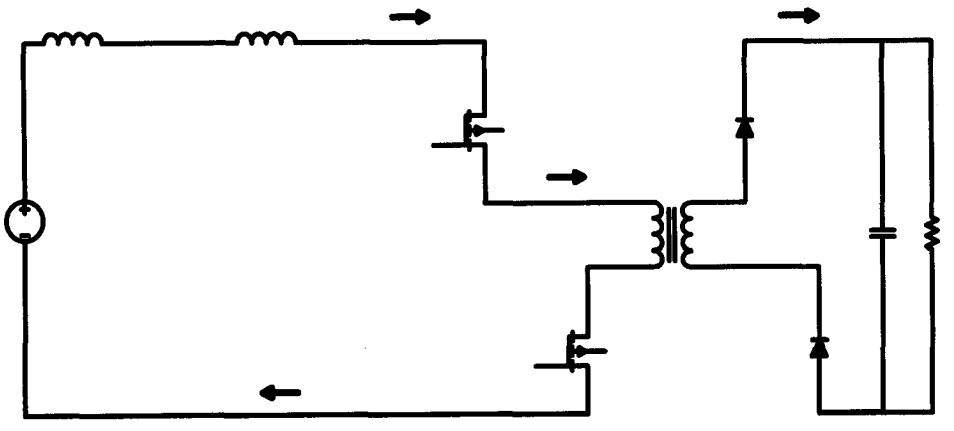

Fig. 2.4(i) Current flow in Mode 8

2.3 Conclusion

In this chapter a new auxiliary circuit for ZCS-PWM full-bridge converters was proposed. The basic operation of a full-bridge boost converter with the proposed auxiliary circuit was shown along with the current and voltage waveforms of different circuit components during different stages or modes of operation of the converter in steady state over a switching cycle. From the discussions presented in this chapter it can be seen that the proposed boost converter operates as a PWM DC-DC boost converter except for the very small instant of time as compared to the whole switching cycle when the auxiliary switch is on facilitating ZCS turn-off of the main switches.

Chapter 3

Circuit Analysis of the Proposed Boost Converter

3.1 Introduction

In the previous chapter, the different modes of steady state operation of a full-bridge boost converter implemented with the proposed auxiliary circuit and operating over a switching cycle were described. In this chapter, an analysis of the boost converter is performed and key mathematical equations are derived based on these modes of operation. These equations are important for understanding the characteristic behavior of the converter with respect to the variation of certain key circuit component values and will help in designing a boost converter with the proposed auxiliary circuit.

3.2 Circuit Analysis

The following assumptions are made regarding different circuit components while analyzing the proposed boost converter topology for analyzing the boost converter circuit:

1) The input inductor is large enough to be considered as a constant current source.

2) The output capacitor is large enough to be considered as a voltage source

3) All semiconductor switches are ideal *i.e* while they are on, they have zero voltage drop across them and that they have no output capacitance across them

4) The reverse recovery time for each diode is zero.

5) The energy feedforward Transformer (T) is ideal *i.e.* it has infinite magnetizing inductance, zero leakage inductance and no lossy components associated with it.

6) From time t_2 to t_4 the auxiliary transformer primary winding is clamped to $V_x = V_o (N_1 / N_2)$ and diode D_{S1} is forward biased, which allows the transfer of the circulating energy from the auxiliary circuit to the output to occur.

7) From time t_4 to t_6 the transformer primary is clamped to $-V_x = -V_o (N_1 / N_2)$ and the diode D_{S2} is forward biased, which allows the transfer of the circulating energy from the auxiliary circuit to the output to occur.

The description of each mode of operation was presented in Chapter 2, and the reader is referred to this chapter for the detailed description of each mode.

The equivalent circuit for Mode 1 is shown in Fig. 3.1. Based on this circuit, the following equation can be derived:

$$V_o N = L_{ik} \frac{di_{in}(t)}{dt} \tag{3-1}$$

where $N = \frac{N_1}{N_2}$

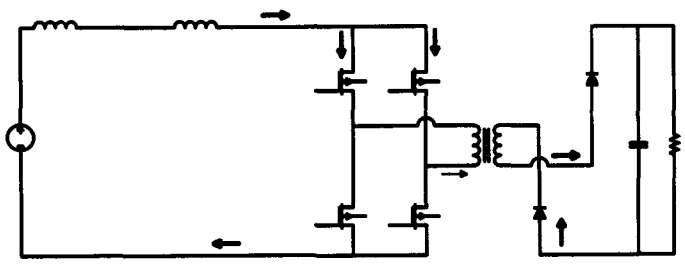

Fig. 3.1 Current flow in mode 1

In this mode, the leakage current L_{ik} drops from I_{in} to zero. Integrating from time t_0 to t_1, $Q_{1,4}$ switches current can be written as

$$I_{Q1\text{-}4}(t) = Iin - \frac{V_o N}{L_{ik}}(t\text{-}t_0) \qquad \text{for time } t_0<t< t_1 \qquad (3\text{-}2)$$

The converter enters Mode 2 ($t = t_1$) of operation when the auxiliary switch Q_{aux} is turned on and C_r begins to resonate with L_{r2} and discharge. The transformer primary voltage is clamped to $V_x = V_o \frac{N_1'}{N_2'}$ from time t_2 to t_4 and the secondary diode D_{s1} is forward biased.

The equivalent circuit diagram for this mode is shown in Fig. 3.2, which can be simplified in Fig 3.4.

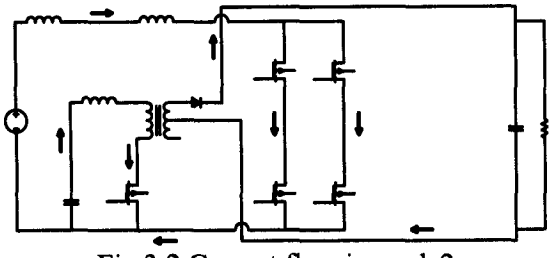

Fig.3.2 Current flow in mode2

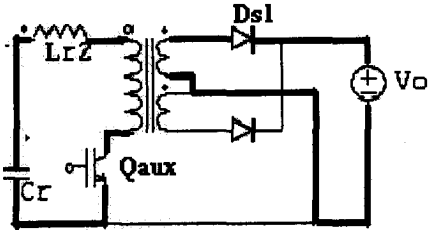

Fig.3.3 Current flow in active part of auxiliary circuit in mode2

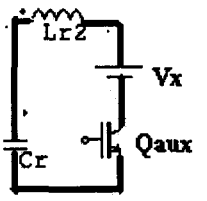

Fig.3.4 Reduced equivalent circuit of the auxiliary circuit in mode2

Voltage V_{Cr} and current I_{Lr2} can be expressed according to the following equations:

$$V_{Cr}(t) = L_{r2}\frac{di_{Lr2}(t)}{dt} + V_x \tag{3-3}$$

$$i_{Lr2}(t) = i_{Cr}(t) = -C_r\frac{dV_{Cr}(t)}{dt} \tag{3-4}$$

$$V_{Cr}(t) = -L_{r2}C_r\frac{d^2}{dt^2}V_{Cr}(t) + V_x \tag{3-5}$$

The differential equation (3-5) has the following initial conditions: $V_{cr}(0)$ is the initial capacitor voltage for this mode and $V_{cr}'(0)$ is the initial time derivative of the capacitor voltage for this mode. Since the initial current in L_{r2} is zero, therefore equation (3-6) can be written as

$$[\frac{d}{dt}V_{Cr}(t)]_{t=0} = -(1/C_r)[\frac{d}{dt}q_{Cr}(t)]_{t=0} = (1/C_r)[\,i_{Lr2}(t)]_{t=0} = 0 \tag{3-6}$$

and the solution to this equation is

$$V_{Cr}(t) = V_x + (V_{Cr}(0) - V_x)\cos\omega_2 t \quad \text{for} \quad t_2 < t < t_3 \tag{3-7}$$

From the initial conditions of Mode 2, $i_{Lr2}(t) = i_{Cr}(t)$ for $t_2 < t < t_3$ and

$$i_{Lr2}(t) = i_{Cr}(t) = -C_r\frac{d}{dt}V_{Cr}(t) = C_r(V_{Cr}(0) - V_x)\omega_2\sin\omega_2 t$$

$$= [(V_{Cr}(0) - V_x)/Z_2]\sin\omega_2 t \text{ for } t_1 < t < t_2 \tag{3-8}$$

where $\omega_2^2 = 1/ L_{r2}C_r$ and $Z_2 = \sqrt{Lr2/Cr}$ is characteristic impedance of the auxiliary circuit. Since this mode ends when the voltage across Cr is zero, the duration of this mode can be determined from equ.(3-7) to be

$$t_2\text{-}t_1 = [\cos^{-1}(-V_x/(V_{Cr}(0)\text{-}V_x)]/\omega_2 = \gamma \qquad (3\text{-}9)$$

so that

$$i_{Lr2}(t) = i_{Lr2}(t_4) = [(V_{Cr}(0)\text{-}\ V_x)/Z_2]\ \sin\omega_2\ \gamma \qquad (3\text{-}10)$$

At the end of Mode 2, since $V_{Cr}(0) >> V_x$, then $\gamma \approx \pi/2$ according to equation (3-9) and (3-10) can be approximated as:

$$i_{Lr2}(t_4) \approx (V_{Cr}(0)\text{-}\ V_x)/Z_2 \qquad (3\text{-}11)$$

Mode 3 of the operation starts at t_2 when D_{aux} starts conducting. The equations that define this mode also define Modes 4 and 5; this can be seen by considering the equivalent circuit diagrams for each mode. Fig 3.5 shows the equivalent circuit diagram of Mode 3 and the reduced equivalent circuit diagram for this mode is shown in Fig. 3.6. Similar diagrams are shown in Figure 3.7 and 3.8 for Modes 4 and 5.

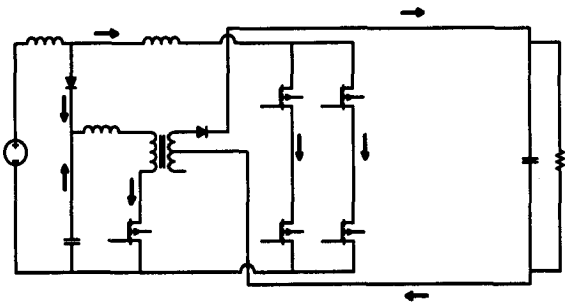

Fig. 3.5 Current flow during mode 3

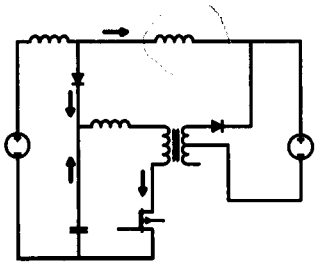

Fig.3.6 Reduced equivalent circuit of mode 3

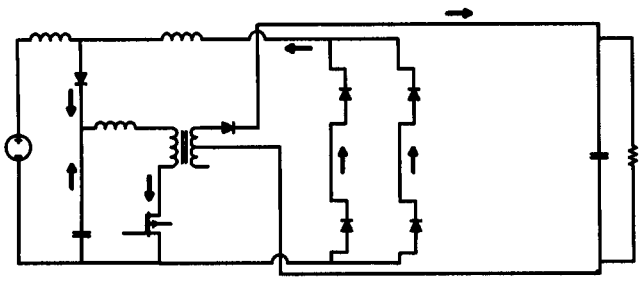

Fig. 3.7. Flow of current in mode 4

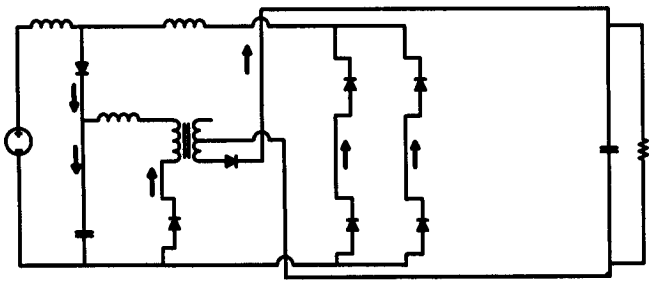

Fig. 3.8. Current flow in mode 5

It can be seen from Figures 3.5 to 3.8 that the flow of current is not interrupted by any switching action so that it is continuous; therefore Modes 3-5 can be considered as a single mode of operation for the purpose of analysis.

By applying Kirchoff's current law to the equivalent circuit in Fig.3.8, the following relation is found:

$$I_s=i_{Lr1}(t)+i_{Lr2}(t)+i_{Cr}(t) \quad (3\text{-}12)$$

The initial conditions for the combined modes are $i_{Lr1}(t_3)=I_s$, $V_{Cr}(t_3)=0$ and

$$i_{Lr2}(t_3)\approx(V_{Cr}(0)- V_x)/Z_2 \quad (3\text{-}13)$$

Since diode D_2 is conducting, the following equation can be written:

$$V_{Lr1}=V_{Cr}=V_{Lr2}+V_x \quad (3\text{-}14)$$

Differentiating equation (3-12) with respect to time gives the following:

$$0=\frac{d}{dt} i_{Lr1}(t)+\frac{d}{dt} i_{Lr2}(t)+\frac{d}{dt} i_{Cr}(t) \quad (3\text{-}15a)$$

The time derivative of I_{in} is zero because it is the input current, which is assumed to be constant when the auxiliary circuit is active. Substituting equation (3-14) in equation (3-15a) results in

$$0=V_{Cr}(t)/L_{r1}+[V_{Cr}(t)-V_x]/L_{r2}+C_r\frac{d^2}{dt^2} V_{Cr}(t) \quad (3\text{-}15b)$$

which can be rewritten as

$$0= V_{Cr}(t)/L_{eq}-V_x/L_{r2}+C_r\frac{d^2}{dt^2} V_{Cr}(t) \quad (3\text{-}15c)$$

where $L_{eq}=L_{r1}L_{r2}/(L_{r1}+L_{r2})$. Equ. (3-15c) can be rearranged to give

$$- C_r\frac{d^2}{dt^2} V_{Cr}(t)= V_{Cr}(t)/L_{eq}-V_x/L_{r2} \quad (3\text{-}15d)$$

Dividing both sides of (3-15d) by C_r results in

$$-\frac{d^2}{dt^2} V_{Cr}(t)= V_{Cr}(t)/L_{eq}C_r - V_x/L_{r2}C_r \quad (3\text{-}15e)$$

Substituting $\omega_{eq}^2= 1/L_{eq}C_r$ and $\omega_2^2=1/L_{r2}C_r$ into this equation gives

$$-\frac{d^2}{dt^2} V_{Cr}(t) = V_{Cr}(t)\omega_{eq}^2 - V_x\omega_2^2 \qquad (3\text{-}15f)$$

For the combined mode 3-5 of operation, the initial resonance capacitor voltage is

$$V_{Cr}(0)=0 \qquad (3\text{-}16)$$

and its initial time derivative is

$$[\frac{d}{dt} V_{cr}(t)]_{t=0} = -(1/C_r)[\frac{d}{dt} q_{cr}(t)]_{t=0}$$

$$= -(1/C_r)[i_{Lr2}(t)]_{t=0} \approx -(V_{Cr}(0)-V_x)/Z_2C_r \qquad (3\text{-}17)$$

Applying the initial conditions given by (3-16) and (3-17), the solution of the differential equation (3-15f) is given by:

$$V_{Cr}(t)= -[(V_{Cr}(0)-V_x)/\sqrt{(1+Lr2/Lr1)}]\sin\omega_{eq}t + V_x\omega_2^2[1-\cos\omega_{eq}t]/\omega_{eq}^2 \qquad (3\text{-}18)$$

From the equivalent circuit diagrams shown in Figs. 3.5-3.8 the following equation can be written

$$V_{Lr1}(t)=V_{Cr}(t)=L_{r1}\frac{d}{dt} i_{Lr1}(t)= L_{r2}\frac{d}{dt} i_{Lr2}(t)+V_x \qquad (3\text{-}19a)$$

which can be rewritten as

$$V_{Cr}(t)/ L_{r1}=\frac{d}{dt} i_{Lr1}(t) \qquad (3\text{-}19b)$$

and simplified to

$$[V_{Cr}(t)/ L_{r1}]dt=d(i_{Lr1}(t)) \qquad (3\text{-}19c)$$

Integrating from the initial stage t = 0 for this mode to any intermediate time $t<t_6$, then using the initial value of $i_{Lr1}(t)$ and simplifying results in

$$i_{Lr1}(t)=I_S-[(V_{Cr}(0)-V_x)L_{eq}/Z_2L_{r1}][1-\cos\omega_{eq}t]+V_x\omega_2^2[t-\sin\omega_{eq}t/\omega_{eq}]/\omega_{eq}^2L_{r1}$$

for $t_2<t<t_6$ (3-19d)

From equ.(3-19a), it can be written that

$$V_{Cr}(t) = L_{r2}\frac{d}{dt}i_{Lr2}(t)+V_x \quad (3\text{-}20a)$$

Integrating and simplifying this equation with an initial condition of $i_{Lr2}(t)$ approximately equals to $(V_{Cr}(0)-V_x)/Z_2$ which results in

$$i_{Lr2}(t)=(V_{Cr}(0)-V_x)/Z_2-[(V_{Cr}(0)-V_x)L_{eq}/Z_2L_{r2}][1-\cos\omega_{eq}t]+V_x\omega_2^2[t-\sin\omega_{eq}t/\omega_{eq}]/\omega_{eq}^2L_{r2}$$

$$-V_xt/L_{r2} \qquad \text{for } t_2<t<t_6 \quad (3\text{-}20b)$$

At $t = t_6$, the current in the body diodes of the full-bridge switch becomes zero (as shown in Fig. 3.9), and some input current starts to flow through L_{r1}, Q_1 and Q_4. The remaining input current continues to charge C_r and the voltage across it rises. Energy begins to be transferred to the load through D_1 and D_4. At the end of this mode the voltage across C_r charges up to V_{Cr0}.The differential equations describing this mode are

$$I_{in}=C_r\frac{dv_{Cr}(t)}{dt}+i_{Lr1} \quad (3\text{-}21)$$

$$V_{Cr}(t)=L_{r1}\frac{di_{Lr1}(t)}{dt}+\frac{V_o}{N} \quad (3\text{-}22)$$

which have the following initial conditions: $V_{Cr}(0)=Vo/N$, $i_{Lr}(0)=0$, $i_{Cr}(0)=I_{in}$.

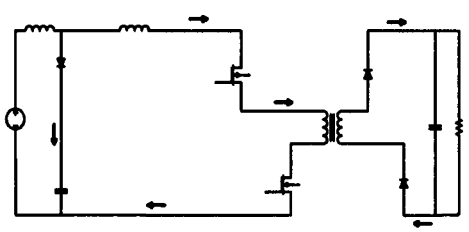

Fig.3.9 Current flow in mode 7

Applying these initial conditions the capacitor voltage in this mode is given by

$$i_{Lr1}(t)=I_{in}(1-\cos\omega_1 t) \tag{3-23}$$

$$V_{Cr}(t)=\frac{Vo}{N}+I_{in}Z_1\sin\omega_1 t \tag{3-24}$$

$$\text{where } \omega_1=\frac{1}{\sqrt{(L_{r1}+L_{lk})C_r}} \tag{3-25}$$

$$\text{and } Z_1=\sqrt{\frac{L_{r1}+L_{lk}}{C_r}} \tag{3-26}$$

where L_{lk} is the transformer leakage inductance.

At the end of this mode the capacitor voltage V_{Cr} reaches its initial value $V_{Cr}(0)$ given by:

$$V_{Cr}(0)=\frac{Vo}{N}+I_{in}Z_1 \tag{3-27}$$

3.3 Summary of Key Equations

In this section the equations describing the current and voltage of different components of the converter during one switching cycle which will prove important for designing circuit components are presented and will be referred while designing a specific boost converter with the proposed auxiliary circuit in Chapter 4.

Initial resonant capacitor voltage $V_{Cr}(0)=\frac{Vo}{N}+I_{in}Z_1$

Resonant capacitor voltage during mode-2: $V_{Cr}(t)= V_x+(V_{Cr}(0)- V_x)\cos\omega_2 t$

Resonant Inductor L_{r2} current during mode-2: $i_{Lr2}(t)= [(V_{Cr}(0)- V_x)/Z_2]\sin\omega_2 t$

Resonant Inductor L_{r2} current during mode-2 to mode-6:

$$i_{Lr2}(t)=(V_{Cr}(0)-V_x)/Z_2-[(V_{Cr}(0)-V_x)L_{eq}/Z_2L_{r2}][1-\cos\omega_{eq}t]+V_x\omega_2{}^2[t-\sin\omega_{eq}t/\omega_{eq}]/\omega_{eq}{}^2L_{r2}$$

$$-V_xt/L_{r2} \qquad \text{for } t_2<t<t_6$$

Resonant Inductor L_{r1} current during mode-2 to mode-6:

$$i_{Lr1}(t)=I_S-[(V_{Cr}(0)-V_x)L_{eq}/Z_2L_{r1}][1-\cos\omega_{eq}t]+V_x\omega_2{}^2[t-\sin\omega_{eq}t/\omega_{eq}]/\omega_{eq}{}^2L_{r1} \qquad \text{for } t_2<t<t_6$$

3.4 Conclusion

In this chapter, the circuit analysis of a PWM dc-dc boost converter operating with an energy feed-forward auxiliary circuit with reduced conduction losses and switch stresses was presented. The various modes of operation that the converter goes through during a switching cycle were presented, and a mathematical analysis of each mode was performed. The results of the analysis will be used to examine the steady-state characteristics in the next chapter of the thesis that will be needed for designing an experimental prototype of such a converter.

Chapter 4

Design Procedure and Example

4.1 Introduction

In this chapter, the results of the mathematical analysis performed on the full-bridge PWM dc-dc boost converter with the proposed auxiliary circuit in the previous chapter will be used to determine the steady-state characteristics and properties of the converter. After these have been determined, they will be used as part of a procedure to design the converter by selecting appropriate converter component values. The procedure will be demonstrated with an example in this chapter and can be used to design other PWM converters with the same auxiliary circuit.

4.2 Conditions for ZCS Turn-Off in the Proposed Full-Bridge Converter

In this section, the conditions for achieving the ZCS of both the main switch and auxiliary switch of the converter with the proposed auxiliary circuit, shown in Fig. 4.1, are analyzed.

The conditions that must be met to ensure the ZCS turn-off of the main switches can be determined from the equations that define the main and auxiliary switch currents during the time that the converter is operating in Modes 3-5, as shown in Chapter 3. These equations are as follows:

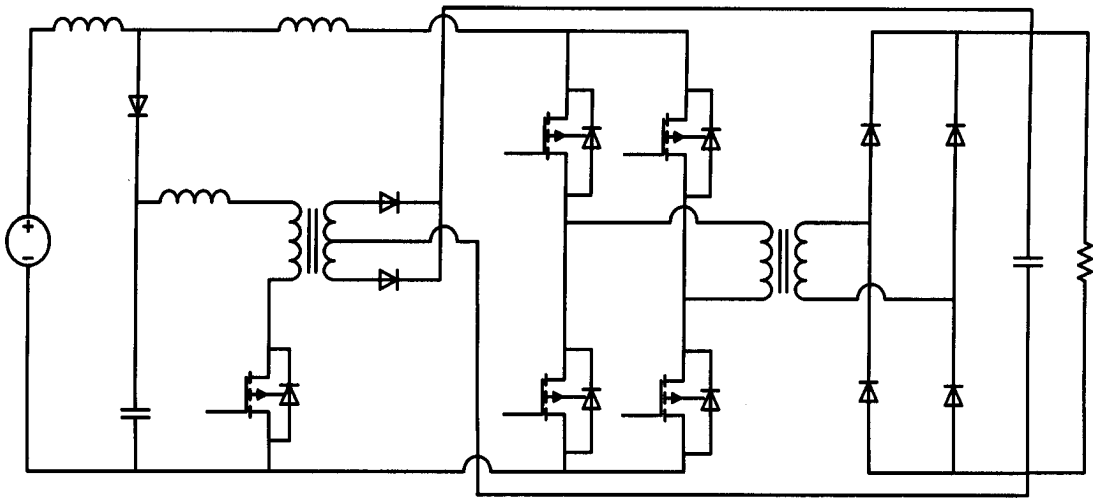

Fig.4.1- PWM DC-DC boost converter with the proposed auxiliary circuit.

$$I_{Q1}(t) = I_s-[(V_{Cr}(0)-V_x)L_{eq}/Z_2L_{r1}][1-\cos\omega_{eq}t] + V_x\omega_2^2[t-\sin\omega_{eq}t/\omega_{eq}]/\omega_{eq}^2L_{r1}$$

$$\text{for } t_2<t<t_6 \qquad (4\text{-}1)$$

$$I_{Qaux}(t)= (V_{Cr}(0)-V_x)/Z_2-[(V_{Cr}(0)-V_x)L_{eq}/Z_2L_{r2}][1-\cos\omega_{eq}t] +$$

$$V_x\omega_2^2[t-\sin\omega_{eq}t/\omega_{eq}]/\omega_{eq}^2L_{r2} -V_xt/L_{r2} \qquad \text{for } t_2<t<t_6 \qquad (4\text{-}2)$$

According to these equations, the currents in the switches can drop to zero, reverse direction, and become negative. A negative value of I_{Q1} in equ. (4-1) represents a flow of current through the body diode of the main switch Q_1 and a negative value of I_{Qaux} in equ. (4-2) represents a flow of current through the body diode of the auxiliary switch Q_{aux}. Since a switch can be turned off with ZCS while current is flowing through its body diode, the key condition that must be satisfied to ensure that a switch can be turned off with ZCS is that the equation that defines its current is negative. This can be done for both Q_1 and Q_{aux} by selecting appropriate values of inductors L_{r1} and L_{r2} and capacitor C_r.

It is evident from equations (4-1) and (4-2) that the instantaneous auxiliary switch current depends mainly on the output voltage, while the instantaneous current of the main switches depends on the output voltage as well as the magnitude of the input current, which can be described by the following equation:

$$I_s = P_o / \eta V_{in} \tag{4-3}$$

where I_s= Input current,

P_o=Output power,

η = Efficiency of the converter,

V_{in}= Input Voltage.

For the current of the main full-bridge switches, if the auxiliary circuit components are properly selected to ensure that the current can become negative for a particular value of $I_{Q1} = I_{Q1,Max}$ (the input current when the converter is operating with maximum load), then the current can become negative for any lesser value of I_{in}, for the same value of V_o. In other words, if a ZCS turn-off for Q_1 can be ensured when $I_{Q1} = I_{Q1,Max}$, then it can also be ensured when $I_{Q1} < I_{Q1,max}$.

To turn off the bridge switches with ZCS under all operating loads, it must be ensured that the auxiliary switch current is greater than the current of the main full-bridge switches during the time that $Q_{1\text{-}4}$ are being turned off, when the converter is operating with maximum load. The peak current of the main switches at maximum load $I_{Q1,max}$ must be less than the peak auxiliary switch current at maximum load, I_{Qaux}, which can be defined as

$$I_{Qaux,max} = (V_{Cr}(0) - V_x)/Z_2 \tag{4-4}$$

where $Z_2=\sqrt{Lr2/Cr}$ is the characteristic impedance of the auxiliary circuit and $Vx=V_o/N$ where N is the turns ratio of the secondary winding to the primary winding of the auxiliary circuit transformer.

Another criterion can be derived by taking the time derivative of equ. (4-2) for the auxiliary switch from time $t_2<t<t_6$. To simplify this analysis, it can be assumed that the auxiliary circuit operates for only a small fraction of the switching cycle. With this assumption, the term

$$V_x\omega_2^2[t-\sin\omega_{eq}t/\omega_{eq}]/\omega_{eq}^2L_{r2}$$

can be neglected so that equ. (4-2) can be written as

$$i_{Qaux}(t) \cong (V_{Cr}(0)-V_x)/Z_2-[(V_{Cr}(0)-V_x)L_{eq}/Z_2L_{r2}][1-\cos\omega_{eq}t]-V_xt/L_{r2} \qquad (4\text{-}5)$$

for time $t_2<t<t_6$. If the same assumption is applied to equ. (4-1), then it can be written as

$$i_{Q1}(t) = I_s-[(V_{Cr}(0)-V_x)L_{eq}/Z_2L_{r1}][1-\cos\omega_{eq}t] \quad \text{for time } t_2<t<t_6 \qquad (4\text{-}6)$$

The time at which i_{Qaux} is at its minimum value, T_{ms2}, can be determined by differentiating and simplifying equ. (4-5) with respect to time and equating it to zero

$$T_{ms2} = (1/\omega_{eq})\sin^{-1}[-\{V_x/(V_{Cr}(0)-V_x)\}\sqrt{(1+Lr2/Lr1)}] \qquad (4\text{-}7)$$

The currents in all switches at time T_{ms2} given by equ. (4-7) must be less than or equal to zero to achieve ZCS for all switches $Q_{1\text{-}4}$ and Qaux. By replacing the value of T_{ms2} given by equ.(4-7) in the equation for i_{Q1}, equ. (4-1), and solving for $i_{Q1}(t)=0$, the following condition for the ZCS turn-off of Q_1 can be determined after subsequent simplifications:

$$[I_sZ_2(L_{r1}+L_{r2})/L_{r2}][2(V_{Cr}(0)-V_x)-I_sZ_2(L_{r1}+L_{r2})/L_{r2}] \geq V_x^2(1+L_{r2}/L_{r1}) \quad (4\text{-}8)$$

This condition can be further simplified so that a ZCS turn-off of $Q_{1\text{-}4}$ can be ensured if the following two simpler conditions are met

$$2(V_{Cr}(0)-V_x)L_{r2}/I_sZ_2(L_{r1}+L_{r2})>1 \quad (4\text{-}9)$$

$$2I_sZ_2(V_{Cr}(0)-V_x)/V_x^2>1 \quad (4\text{-}10)$$

These conditions can be met by the proper selection of the appropriate circuit component values. A similar condition for the ZCS turn-off of Q_{aux} can be derived by substituting the value of T_{ms2} derived in equ. (4-7) into equ. (4-2)

$$(V_{Cr}(0)-V_x)/Z_2-(V_{Cr}(0)-V_x)/Z_2\left[1+\sqrt{1+\{V_x^2/(V_{Cr}(0)-V_x)\}\left(1+Lr2/Lr1\right)}\right] < V_x/L_{r2}\omega_{eq} \quad (4\text{-}11)$$

Another important factor that must be considered when designing the converter is the peak current in the auxiliary switch. When designing the auxiliary circuit, the peak current in the auxiliary switch should be reduced to decrease the stresses on the devices.

4.3 Characteristics of the Proposed Full-Bridge Converter

The equations for the modes of operation that were presented in Chapter 3 for the full-bridge PWM dc-dc boost converter with the proposed auxiliary circuit (Fig. 4.1) can be used to generate graphs of steady-state characteristic curves for this converter.

The graphs can be generated by a computer program such as the MATLAB program presented in Appendix A of this thesis. The key to the program is the fact

that, since it is the steady-state characteristics that are to be determined, the current and voltage of any converter component at the start of a switching cycle must be the same as that at the end of a switching cycle. If the equations derived in the previous chapter are used by the computer program to track component current and voltage values throughout a switching cycle when the converter is operating with a given set of component values, then the program can determine if the converter is operating in steady-state. Once this has been determined, then the appropriate steady-state component voltage and current values can be found. If this is done for a number of component value sets, then characteristic curves and graphs can be generated.

The characteristic graphs that are generated and shown, show the effects that changing a particular component value, such as that of a particular inductor or a capacitor, can have on converter currents and voltages. With these graphs, it then becomes possible to develop a systematic procedure for the design of the converter that would allow appropriate converter component values to be selected.

Graphs of steady-state characteristic curves are shown in Figs. 4.2-4.4. The curves were generated for the following operating condition:

Output Voltage V_o=300Volts

Output Power P_o=600Watts

Input Voltage Vin=24Volts

Expected Efficiency $\acute{\eta}$= 93%

Switching Frequency=f_s=1/T_s=50 kHz.

The design procedure that is presented is an iterative one and requires several iterations before the final design can be completed. It should be noted that only the design of the auxiliary circuit components is presented here since that of the main power circuit can be found in any standard power electronics textbook. The design of the main power transformer, however, is dependent on the PWM method used to control this converter and will be discussed in the following steps.

Step 1: Minimize reverse recovery losses in the auxiliary diode

The duration of Mode 7 in which the input current gets diverted from the auxiliary capacitor C_r to the inductance L_{r1} should be greater than $3*t_{rr}$ (reverse recovery time) for auxiliary diode. The factor $3*t_{rr}$ is a typical duration of time needed to gradually transfer away from the diode so that the diode can stop conducting current with little, if no, reverse recovery time; this is typically 3*80ns=240ns. The expression for the commutation time t_c can be found from eqn. (3-23) as:

$$t_c = \frac{\pi}{2\omega_1} \tag{4-12}$$

$$\text{where } \omega_1 = \frac{1}{\sqrt{(L_{r1}+L_{lk})C_r}} \tag{4-13}$$

by combining eqns. (4-12) and (4-13), eqn. (4-14) can be written as:

$$t_c = \frac{\pi}{2}\sqrt{(L_{r1}+L_{lk})C_r} \tag{4-14}$$

The value for the commutation time t_c in which the input current gets diverted from the auxiliary capacitor C_r to the bridge section, must be greater than the value of 3trr of the auxiliary diode. So from this discussion the following relation can be derived:

$$3t_{rr}=t_c=\frac{\pi}{2}\sqrt{(L_{r1}+L_{lk})C_r}=240nS \qquad (4\text{-}15)$$

Eqn. (4-15) will be used along with equations derived in the following steps to determine values of C_r and L_{r1}.

Step 2: Determine the values of C_r and L_{r1}

In this step, the values of C_r and L_{r1} are determined. Referring to Mode7 when switches Q_2 and Q_3 are turned off and voltage across them builds up due to resonance between the equivalent series inductance of leakage inductance L_{ik} and L_{r1} and capacitor C_r. At the end of this mode the voltage across the switches rises to a certain peak voltage given by eqn. (3-27):

$$V_{Cr}(0)=\frac{Vo}{N}+I_{in}Z_1$$

The value of this peak voltage across the switches, which is same as the maximum voltage across the resonant capacitor, is plotted for different values of impedance Z_1 in Fig.4.2. It can be found from this graph that by choosing a larger impedance, the voltage across C_r will increase. If a smaller impedance is chosen, then a larger capacitor must be used for C_r as there must be enough energy stored in the

capacitor at the end of this mode to force the current into the full bridge to reverse direction and create an opportunity for the ZCS turn off of switches.

By choosing a large capacitor, the resonance cycle time will increase in the circuit which in turn will increase the on-time duty ratio in the auxiliary switch and will cause more losses as the device has to be on longer. The energy in the capacitor is $\frac{1}{2}CV^2$, so either a higher voltage can be placed across the capacitor or a bigger capacitor can be chosen. For this design, a value of Z_1=1.5 Ω is chosen. Using eqn. (4-13) determined in Step 2 and Z_1 given by eqn. (3-26) in this step, values of L_{r1} and C_r are found to be 240nH and 360nF by assuming L_{ik} to be typically around 500nH.

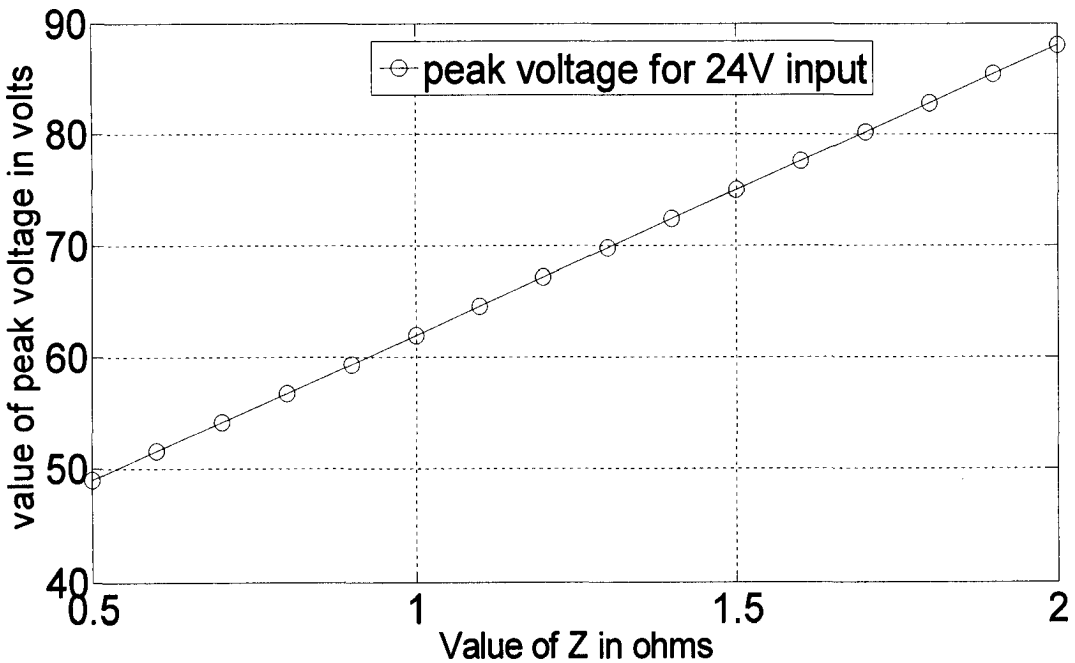

Fig.4.2 Variation of capacitor C_r Peak voltage for different values of Z_1

Step 3: Determine the characteristic impedance of the auxiliary circuit and the value of L_{r2}.

The characteristic impedance of the auxiliary circuit is defined by:

$$Z_o = \sqrt{\frac{L_{r2}}{C_r}} \tag{4-16}$$

Z_o affects the peak current stress of the auxiliary circuit components and the window of time that the main switches can be turned off with ZCS. It should also be considered that the peak current in the auxiliary switch must be greater than the bridge input current so the bridge current starts reversing and eventually reduces to zero and flow in the opposite direction through the body diodes of the bridge switches which can then be turned off with ZCS.

Low values of Z_o result in higher values of peak current stress, but result in longer windows of time during which the main switches can be turned off with ZCS. It can be seen in Fig. 4.3 that values of Z_o over 1.5 Ω would result in low auxiliary circuit current stresses, but these values of Z_o are unsuitable because the time window for the ZCS turn-off of the main switches would be very narrow or non-existent. Values of Z_o below 1.5 Ω will result in very high peak current in the auxiliary switch, which will increase the losses in it. So for this design, Z_o=1.5Ω is chosen which implies L_{r2}=0.9μH.

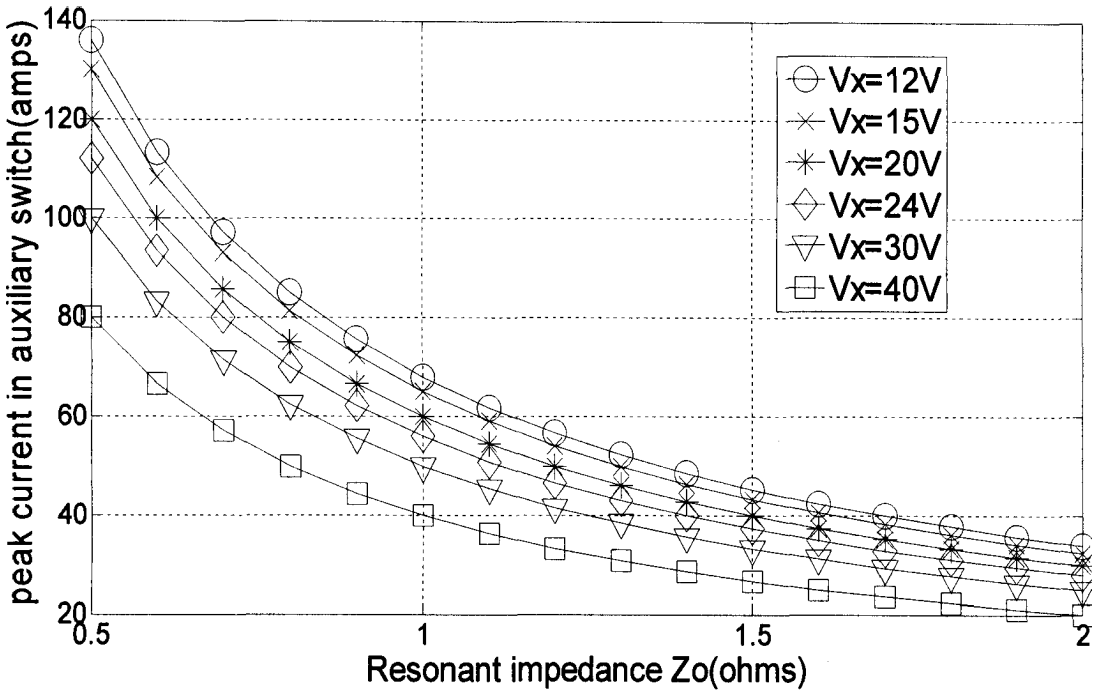

Fig.4.3 Variation of Peak current in auxiliary switch for different values of Z_o

Step 4: Determine the value of N_x

To determine N_x, the effect of the auxiliary transformer secondary voltage on the soft switching window of both auxiliary switch and bridge switches need to be considered. The primary voltage $V_x = V_o/N_x$ across the auxiliary transformer in Modes 2-4 reduces the negative peak voltage across C_r and also reduces peak current across the auxiliary switch. These two phenomena can have a detrimental effect on the ZCS window, but on the other hand they can help in reducing circulating current in the auxiliary circuit.

The characteristic graphs in Figs.4.4 and 4.5 show the effect that V_x has on the duration and amount of negative portion of the bridge switch and auxiliary switch

current for varying values of V_x with other component values decided in previous steps, during Modes 3-5. These are also the modes in which the currents in all switches reduce to zero and reverse directions following eqns. (3-19d) and (3-20b), thus creating ZCS turn off window for the switches.

From the characteristic graph in Fig.4.4, it can be seen that higher the value of V_x lower is the magnitude and duration of the negative portion for the current through the bridge switches. This is expected since with higher values of V_x, the negative peak voltage across C_r is reduced and thus less negative voltage appears across L_{r1} during Modes 3-5, which reduces the duration of its negative current region. On the other hand, it can be seen that the negative part of the auxiliary current is increased with increasing values of V_x since increasing values of V_x will decrease the peak current in the auxiliary switch from which its current starts decreasing. When trying to choose a suitable value for V_x, it should be considered that greater negative switch currents will increase circulating current losses and also increase the duration of activation of the auxiliary circuit, which will also increase conduction losses in it. V_x = 24V or equivalently N_x= 1:12 is chosen considering all these tradeoffs.

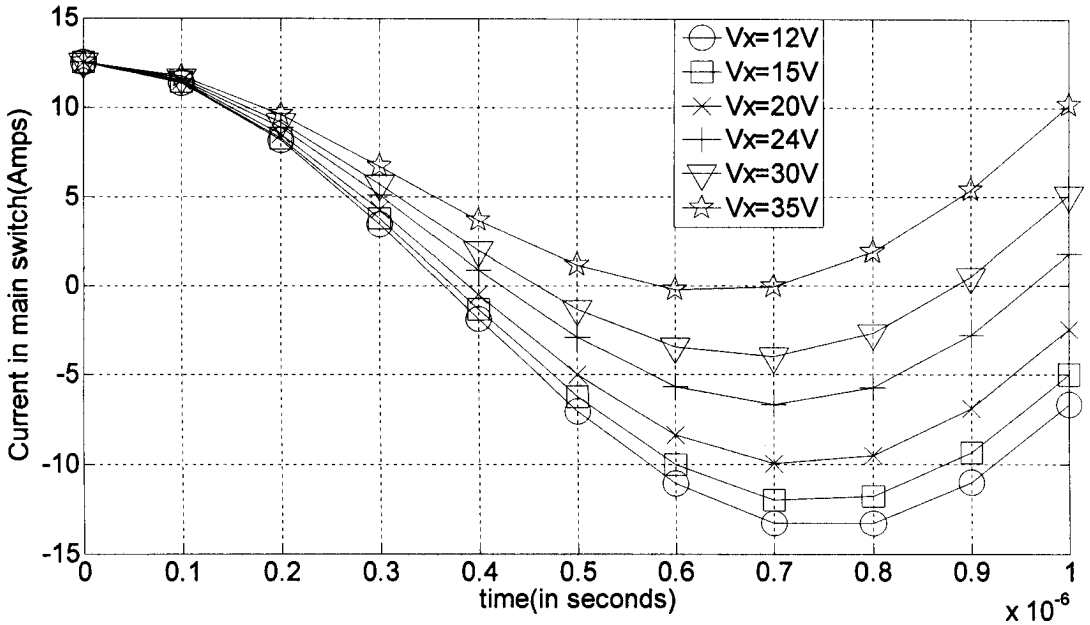

Fig.4.4 Variation of the duration in which bridge switch currents reduce to zero and go negative during Modes 3-5 for different values of N_x.

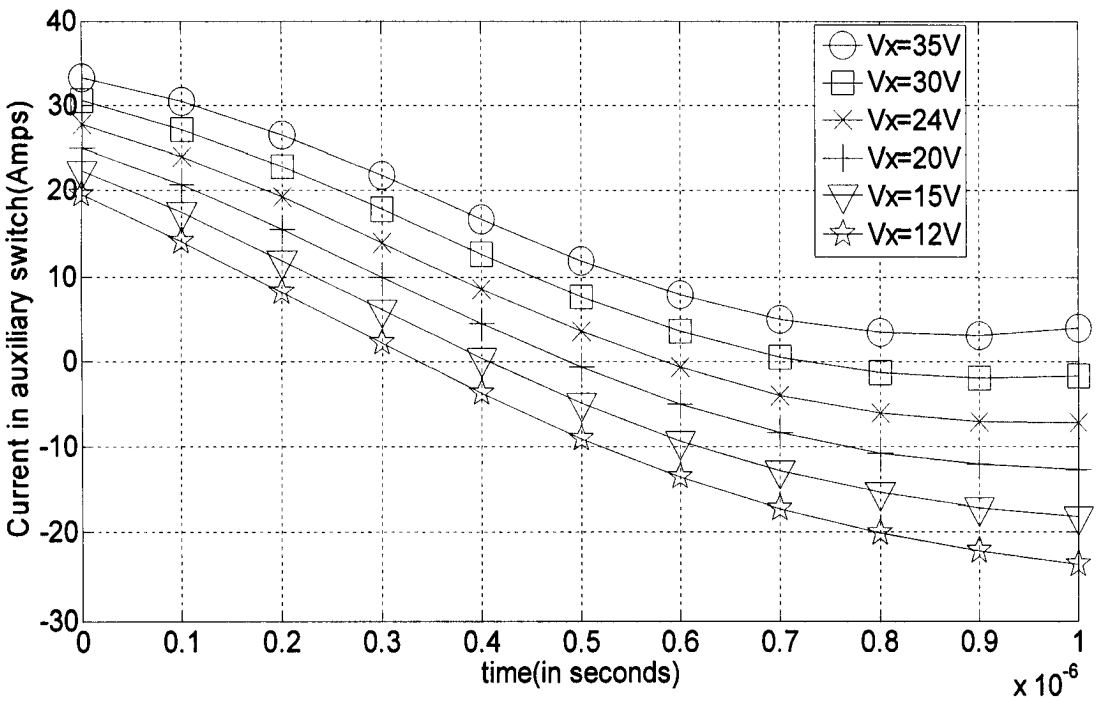

Fig.4.5 Variation of the duration in which bridge switch currents reduce to zero and go negative during Modes 3-5 for different values of N_x.

4.3.1 Design Example

The design of a boost converter operating with the proposed auxiliary circuit is described. For the example, the converter is to be designed according to the following specifications:

Output Voltage V_o=300Volts
Output Power P_o=600Watts
Input Voltage V_{in}=24Volts
Expected Efficiency η= 93%
Switching Frequency=f_s=1/T_s=50 Khz.

4.3.2 Power Circuit Design

The design procedure consists of two parts - the design of the main power circuit (a full-bridge boost converter) and the design of the auxiliary circuit. The first part of the procedure is presented in this section and the second part is presented in the next section.

4.3.3 Designing Input Inductor L_{in}

For full-bridge PWM dc-dc boost converters, the value of input inductance is generally selected to limit the peak-to-peak ripple of the current flowing through the inductor. A compromise must be made when selecting a value for Lin. If L_{in} is too large, then the peak current will be small, but the physical size of the inductor will increase significantly, and so will the size and weight of the converter. A 10% peak-

to-peak (p-p) ripple to average current ratio of the input current is a compromise that is typically made and will also be made in this example. With this compromise, the boost converter is assumed to have a continuous current.

From the given specifications for the converter, the maximum average input current is

$$I_{in}=P_o/V_{in}\eta\approx 27 \text{ Amps.}$$

In this case the p-p ripple of input current is

$$\Delta I= 0.1\ I_{in}= 2.7\text{Amps}$$

Rearranging the conversion ratio for the boost converter given in equation (1-2) to solve for the switch duty ratio D gives

$$D=(V_o-V_{in})/V_o=0.91$$

since $$V_{Lin} = \text{Lin } di/dt \qquad (4\text{-}17)$$

where V_{Lin} is the voltage across L_{in} when switches $Q_{1,4}$ or $Q_{2,3}$ are on; $dt = DT_S$ is the time for which the switch is on and di is the change in input current during that time, the value of Lin can therefore be determined by:

$$\text{Lin}=V_{in}\ DT_S/\ \Delta I= 24\text{Volts}*0.91*20\mu s/2.7\text{Amps}$$

$$= 1.61 \text{ mH.}$$

4.3.4 Designing Output Capacitor C_o

The minimum value of the capacitor can be determined from

$$C_o > D / R_o f_s(\Delta V_o / V_o)$$

given in [MOHAN] where D is the duty ratio determined in equ.(1-1), R_o is the output resistance at maximum load ($V_o^2/P_{o,max}$), fs is the converter switching frequency and ($\Delta V_o/V_o$) is the percentage of peak output voltage ripple. Substituting D = 0.91, fs = 50 kHz, Ro = 150 Ω and $\Delta V_o/V_o = 0.001$, Co can be found to be

$$C_o > D/R_o f_s(\Delta V_o/V_o) = 0.91/(150*50*10^3)*0.001 = 1.22mF.$$

In practice, the filter capacitance value is often determined by the holdup requirements of the supply, not by ripple voltage considerations. This means that starting from an initial bus voltage, the capacitor must store enough energy to maintain the output above a specified minimum voltage, V_{min}, after the input voltage has been absent for a specified time, typically 20ms for worst case design. Assuming that V_{min} is 90% of V_o and T_h is the holdup time, during this holdup time, the energy transferred to the output is $E=p_o*T_h$, which is also equal to the energy discharged by the capacitor is given by:

$$E = C_o(V_o^2 - V_{o,min}^2)/2 \qquad (4\text{-}17)$$

hence C_o is given by:

$$C_o = 2*P_o*T_h/(V_o^2 - V_{o,min}^2) = 2*600*0.02/(300^2 - 270^2) = 1.5mF.$$

4.3.5 Designing Main Switches $Q_{1\text{-}4}$

It can be recalled from Chapter1 that MOSFETs are the device of choice for low power applications and high operating frequencies, for their low cost, ruggedness, and for high switching frequencies.

The average current through the main switch is

$$I_{in}*D=25*0.91=22.75Amps.$$

The peak current flowing through the bridge is the peak current in the input inductor and it is equal to

$I_{Lin,pk} = I_{Lin,avg} + 0.5\ \Delta\ I = 25Amps + 0.5 * 2.7Amps = 26.35Amps$

The maximum voltage across the main switches V_{Q1-4}=75Volts. An "IRF540" device can be selected for the main switches.

4.4 Auxiliary Circuit Design

During Mode 5 in which the input current gets diverted from the auxiliary capacitor Cr to the inductance Lr, must be greater than $3t_{rr}$ (reverse recovery time) for auxiliary diode which is 3*80ns=240ns.

The commutation time is calculated as $t_c = \frac{\pi}{2}\omega_1$ where $\omega_1 = \frac{1}{\sqrt{L_r C_r}}$ and as stated $t_c \geq 3t_{rr}$ so $t_c \geq 240ns$

$$V_{cr} = L_r \frac{di_{Lr}}{dt} + V_p \qquad (4\text{-}18)$$

by solving equ.(4-18) $i_{cr}(t) = I_{in} Cos\omega_1 t = 0$ so $\omega_1 t = \frac{\pi}{2}$

and for a leakage inductance of $0.5\mu H$, $L_{r1} = 0.24\mu H$

In the design procedure $L_{r1} = 0.3\mu H$ is taken and the rest of components will be calculated based on this value.

Fig. 4.6 helps to find out the suitable impedance for the circuit in which the minimum circulating current will be gained and ZCS for all the switches is insured.

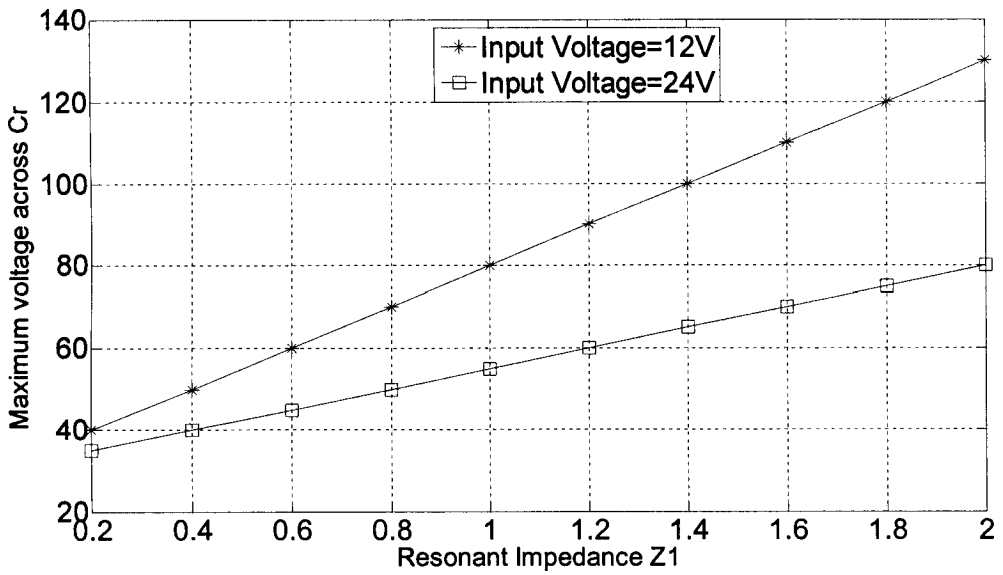

Fig.4.6 Maximum voltage across the auxiliary capacitor vs. resonance impedance of the circuit for input voltages of 12 and 24 Volts

By choosing a larger impedance, the voltage across C_r will increase and by choosing a smaller impedance, a bigger capacitor has to be used in the circuit.

By choosing a big capacitor, the resonance cycle time will increase in the circuit which in turn will increase the on-time duty ratio in the auxiliary switch and will cause more losses as the device has to be on longer. The energy in the capacitor is $\frac{1}{2}C_r V_{Max}^2$, so there is a tradeoff of going high with the voltage or choosing a bigger capacitor.

$$Z_1 = \sqrt{\frac{L_{ik} + L_{r1}}{C_r}} \tag{4-19}$$

and in this particular example $Z_1 = 1.8\Omega$ is chosen.

Knowing Z_1, L_{r1} and L_{ik}, the value of C_r can be determined by solving eqn.(4-19) for C_r and finding C_r =350nf. (In the practical experience we are using a 0.36uf standard ac capacitor)

Fig. 4.7 shows the current in the auxiliary switch when the voltage in the capacitor has reduced to zero. To ensure ZCS in the circuit, the peak current in the switches has to be bigger than the current flowing into the bridge, so the current will flow back from the bridge and ZCS is insured.

An impedance value of about 1.5 ohms has been taken from the characteristic graph as it is very important that the peak current always be larger than the current in the bridge (25-30Amps).

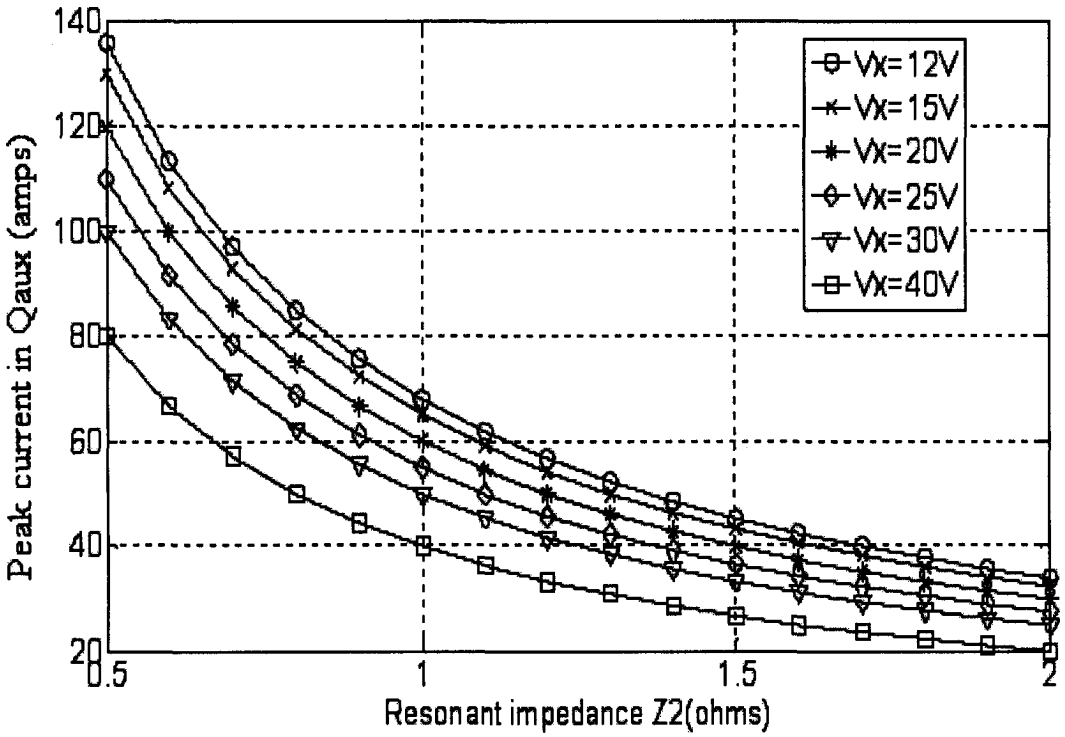

Fig.4.7 Peak current in the auxiliary switch vs. Resonance impedance

Knowing Z_2=1.5Ω and C_r =350nf, L_{r2} can be found from the equation below,

$$Z_2 = \sqrt{\frac{L_{r2}}{C_r}} = 0.88\text{uH}$$

There is also another way to confirm the value of L_{r2} calculated above and it is based on the ratio between L_{r2} and L_{r1} which can be determined from Figures 4.8(a) and 4.8(b).

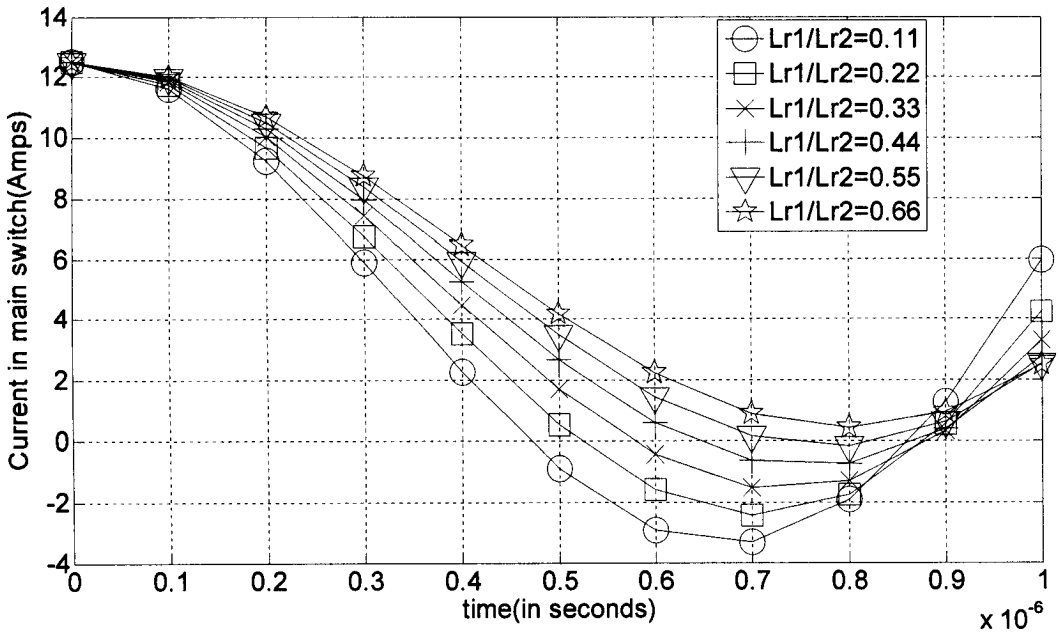

Fig 4.8(a). Current flowing through the main switches for different ratios of L_{r1}/L_{r2}

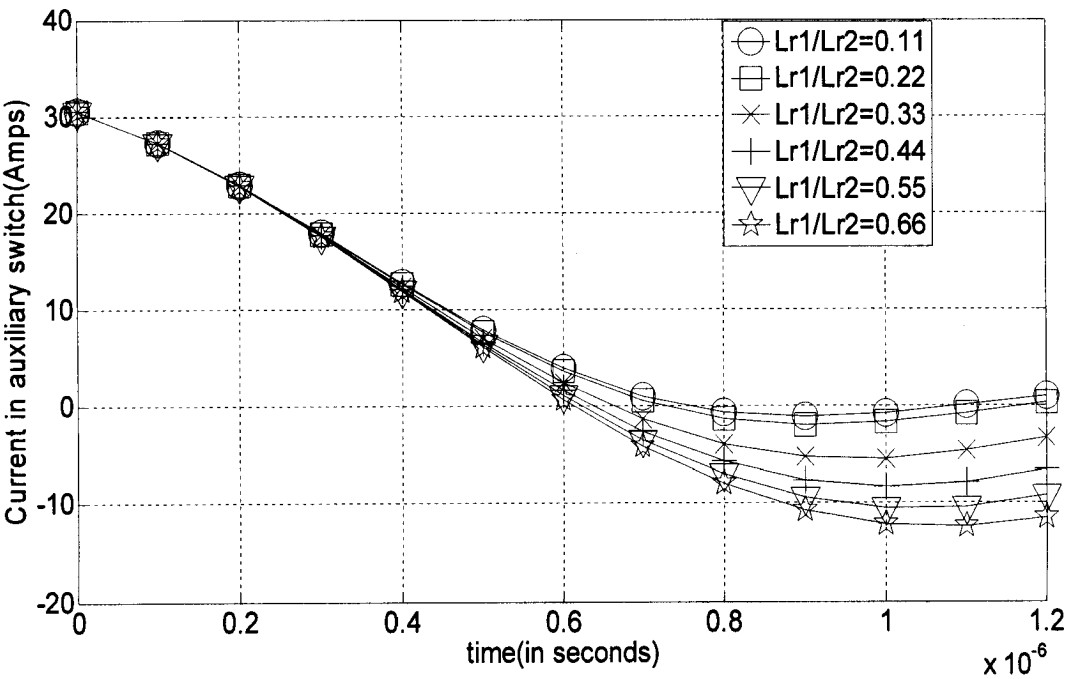

Fig 4.8(b). Current flowing in the auxiliary switch for different ratios of L_{r1}/L_{r2}

In these graphs, current in the main switches and the auxiliary switch have been shown for different ratio amounts of L_{r1}/L_{r2}. A curve that ensures ZCS operation has to be chosen, whereas the ones with a huge negative peak should not be considered as this signifies high circulating current, which results in more conduction losses. By analyzing both graphs, $L_{r1}/L_{r2}=0.33$ looks the best choice because it has a proper negative peak current in both graphs that will ensure the ZCS operation while the peak is not so big to cause more conduction losses.

4.5 Simulation Results

With the values of resonant inductances, capacitance and the transformer turns ratio the converter circuit was simulated in the circuit simulator PSIM. The following figures show the simulation waveforms generated by the PSIM circuit simulator, and a table of the current and voltage of different circuit components determined by PSIM simulation results are also given. The PSIM results help in verifying the choice of all devices for the specified converter. Key simulation results can be compared with the experimental results in chapter 5.

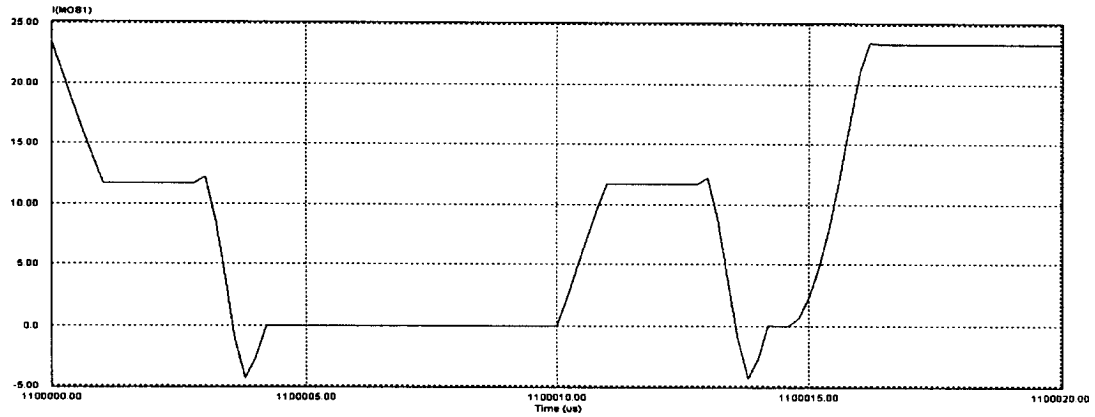

Fig. 4.9 PSIM simulation of main switches $Q_{1,4}$ currents

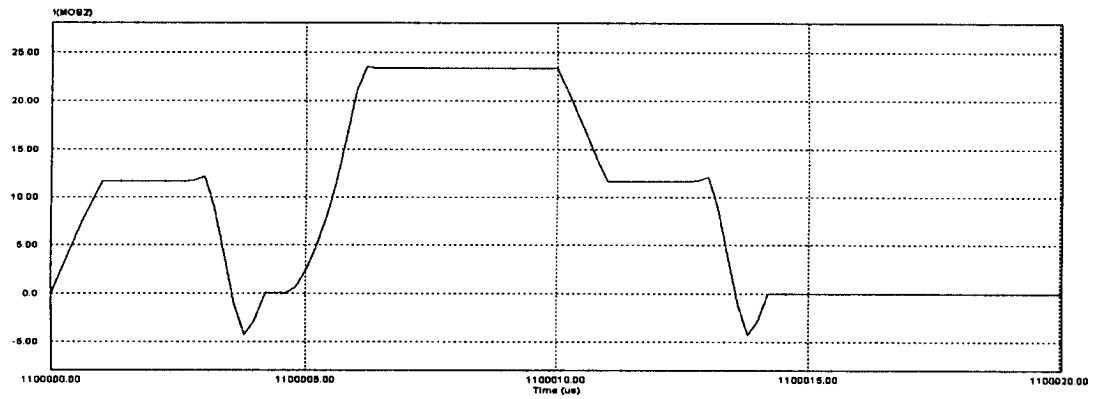

Fig. 4.10 PSIM simulation of Main switches $Q_{2,3}$ Currents

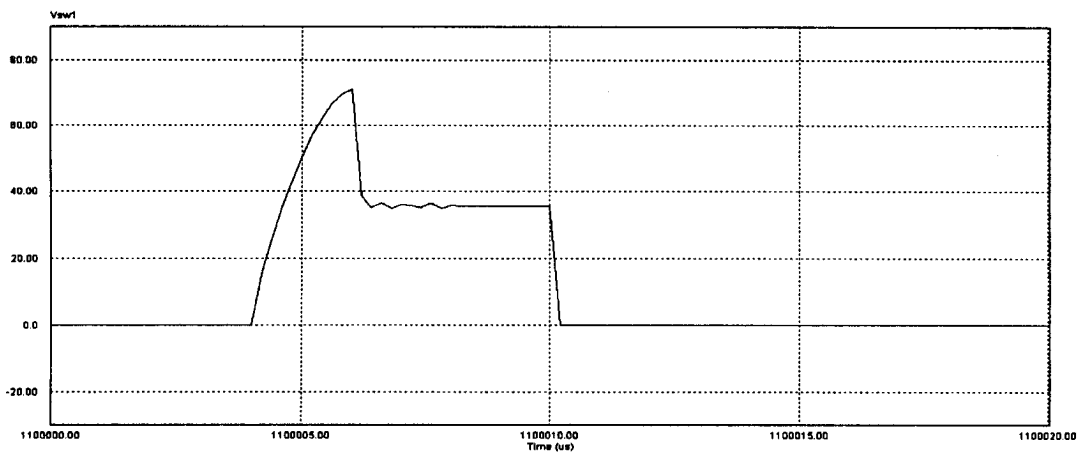

Fig 4.11 PSIM simulation of the voltage across Q_1 and Q_4

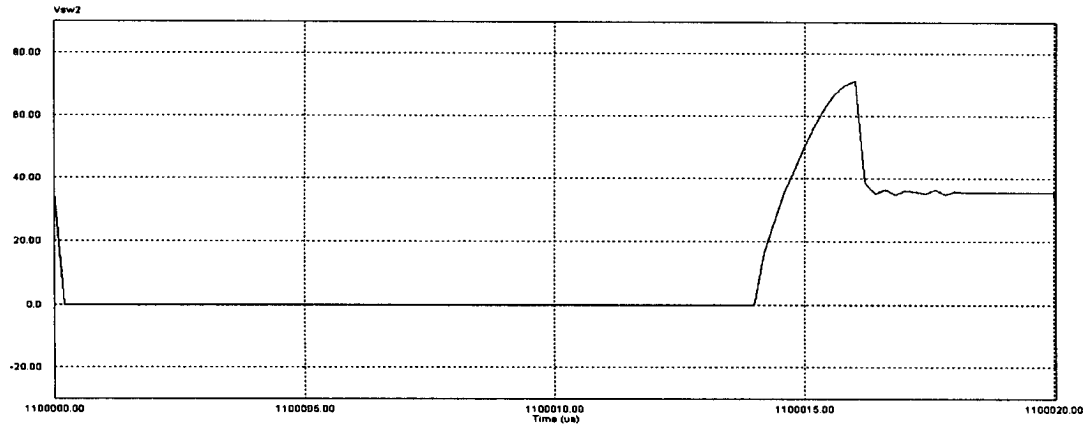

Fig 4.12 PSIM simulation of the voltage across Q_2 and Q_3

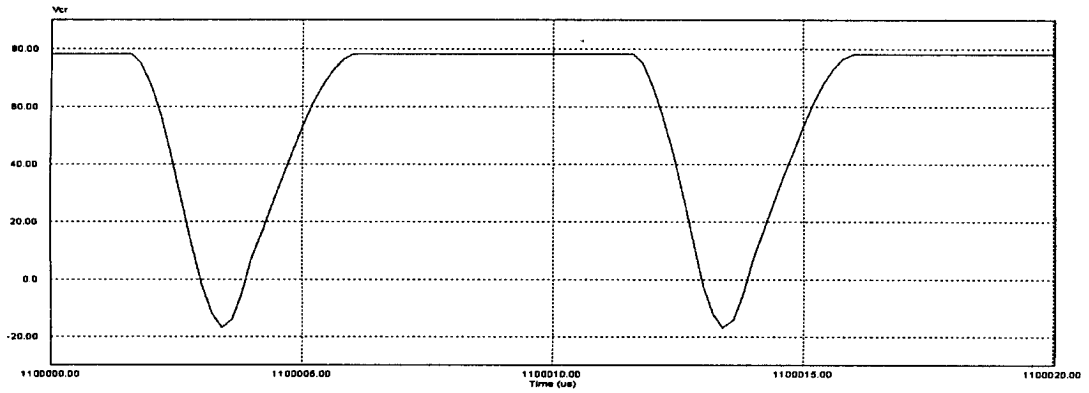

Fig.4.13 PSIM simulation of resonant capacitor voltage

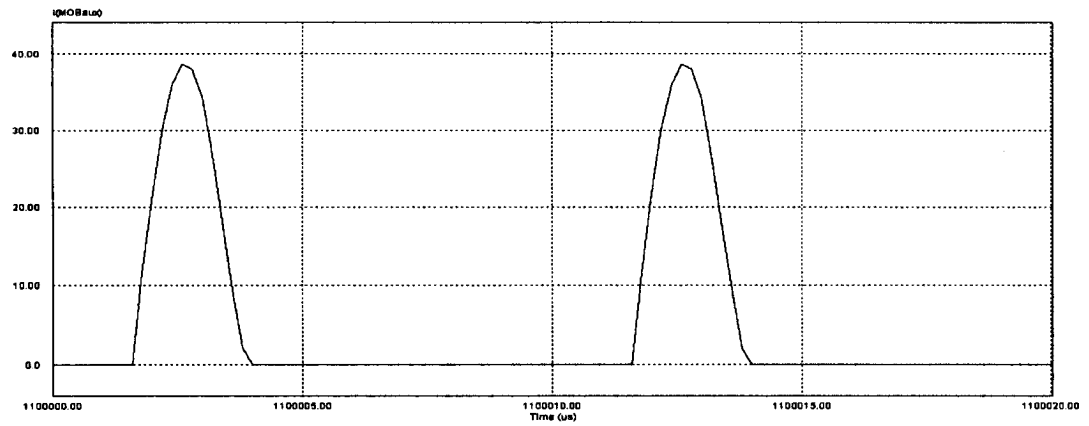

Fig.4.14 PSIM simulation of auxiliary switch current

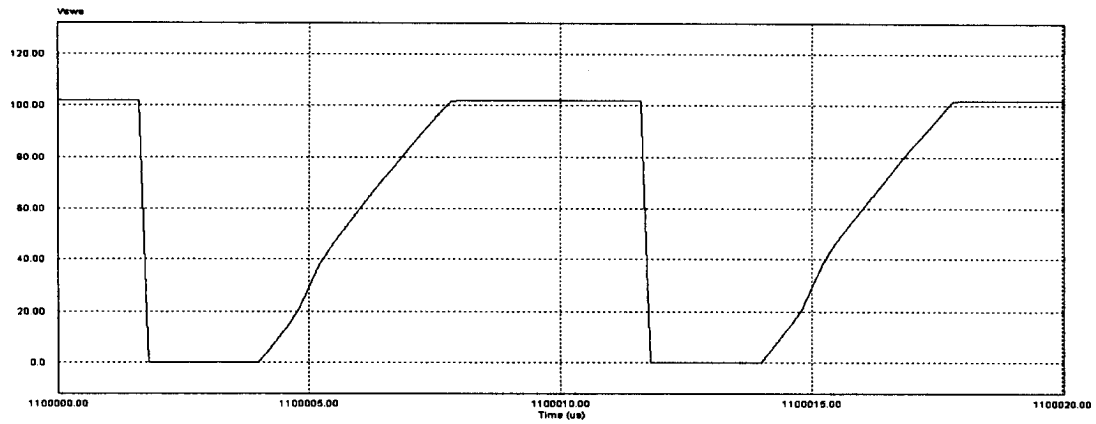

Fig.4.15 PSIM simulation of the voltage across Q_{aux}

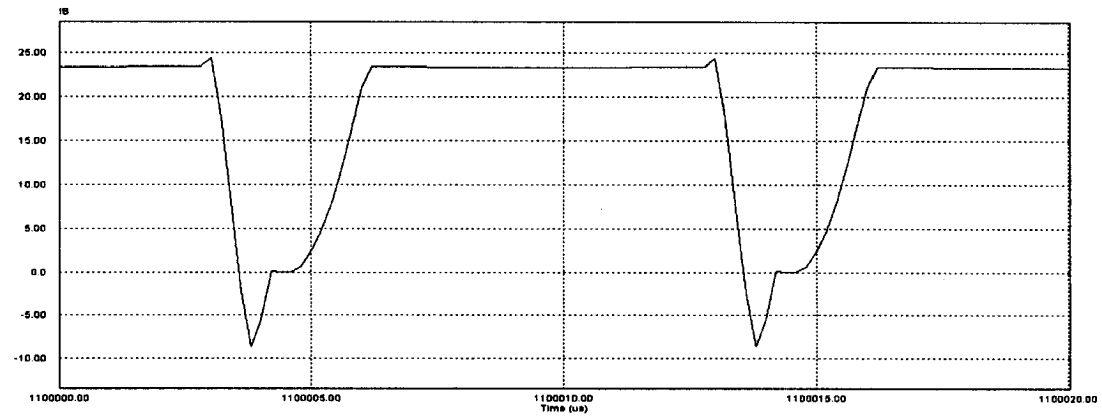

Fig.4.16 PSIM Simulation of the bridge input current I_{Lr1}

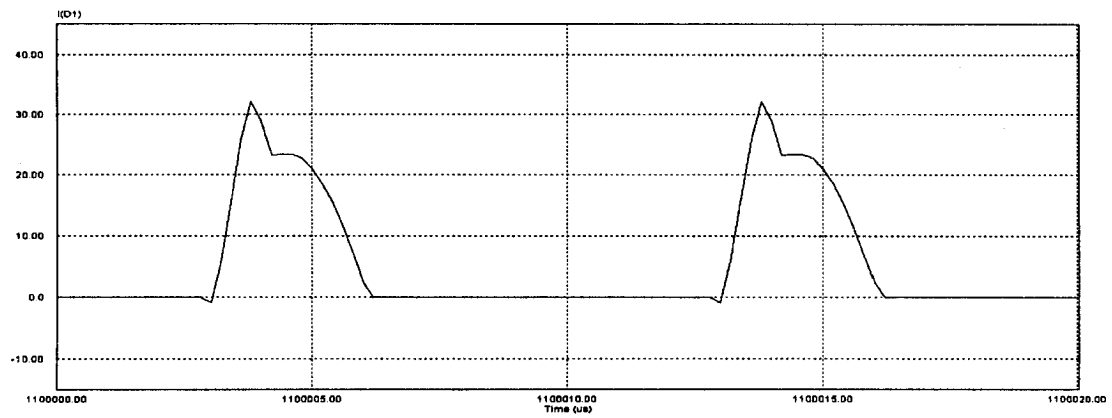

Fig.4.17 PSIM simulation of auxiliary diode current

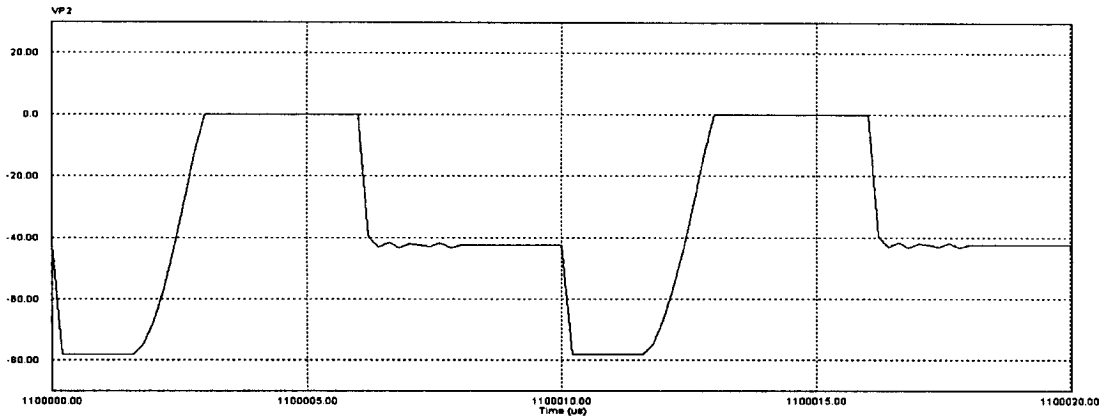

Fig.4.18 PSIM simulation of the auxiliary diode voltage

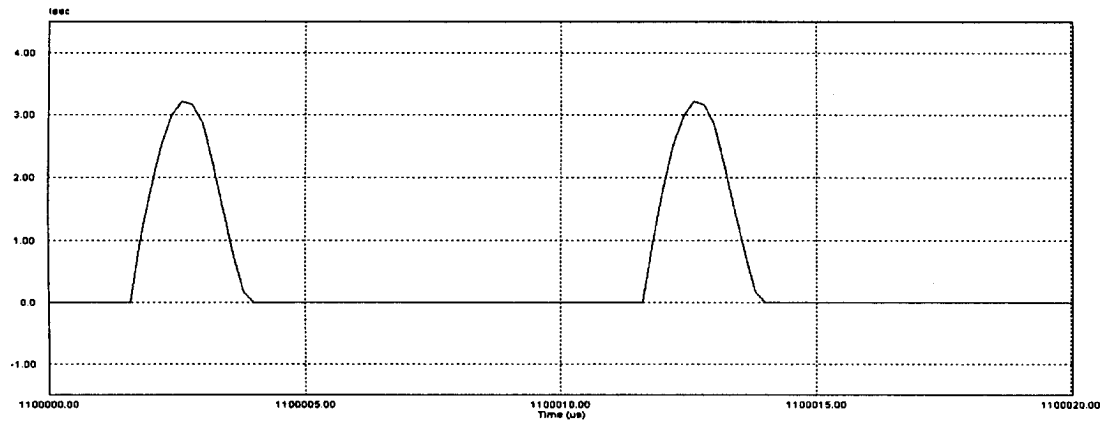

Fig.4.19 PSIM simulation of the auxiliary transformer secondary current

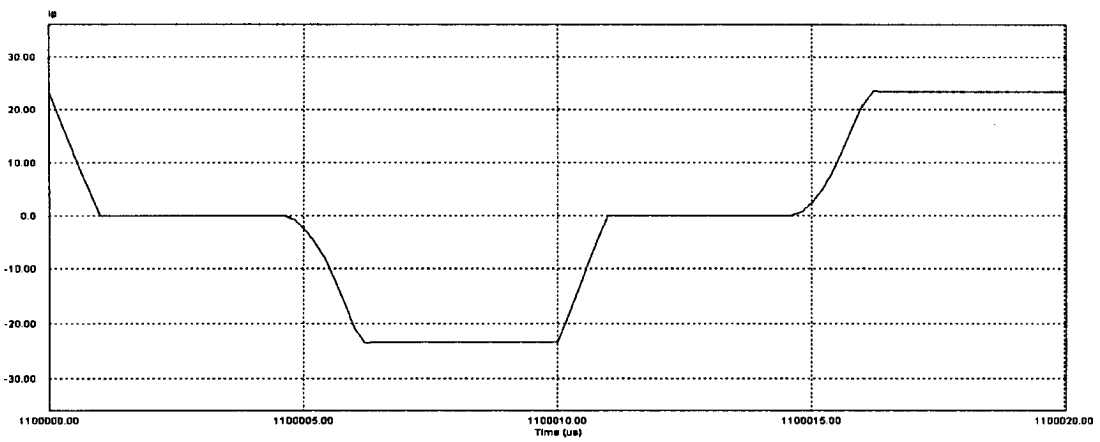

Fig.4.20 Input current in transformer T

4.6 Conclusion

In this chapter, the results of the mathematical analysis performed in the previous chapter on the PWM dc-dc boost converter with the proposed auxiliary circuit were used to determine the steady-state characteristics and properties of the converter. This was done by using a MATLAB program that determined steady-state auxiliary circuit voltages and current characteristics over a switching cycle for various sets of component values, and that determined the effect that individual circuit parameters had on converter operation. The results of the MATLAB program and circuit simulator PSIM were plotted as graphs, which were then used as part of a design procedure.

Chapter 5
Experimental Results

5.1 Introduction

In this chapter, results obtained from an experimental full-bridge PWM dc-dc boost prototype converter operating with the dual auxiliary circuit examined in the previous chapters of this thesis are presented. The converter was implemented with the same parameters as the ones selected in the design example of Chapter 4. Typical converter waveforms are shown as well as efficiency results. Various observations of the experimental results are stated and explanations are given.

5.2 Experimental Results

The feasibility of a PWM dc-dc boost converter operating with the example dual auxiliary circuit discussed in Chapters 3 and 4 was verified by an experimental Proto type that was designed according to the following specifications:

Output Power: $P_o = 600W$

Output voltage: $V_o = 300V$

Input Voltage: $V_{in} = 24V$

Switching frequency: $f_{sw} = 50kHz$

The prototype was implemented with the parameters from the design example discussed in the previous chapter. A saturable reactor implemented with 5 turns on a Toshiba saturable core L_S (SA14x8x4.5) was used to reduce possible voltage overshoots and ringing that can be caused by parasitic elements in the circuit.

The following components were used to implement the boost converter prototype with the proposed auxiliary circuit:

1) Input Inductance L_{in}: 500μH /Mu 77194A7
2) Main Bridge Switches Q_{1-4}: IRF540
3) Output Capacitor: 3X360μF 3316(M)
4) Auxiliary Switch: IRF520IR
5) Auxiliary Diode: FR802
6) Resonant inductor L_{r1}: 300nH /3 Turns on 1402D 55894A2 0 core
7) Resonant Inductor L_{r2}: 900nH/ 5 Turns on 1402D 55894A2 0 core
8) Energy Feed Forward Transformer: 1:12 turns on 6832E 7753A7 core
9) Main Bridge Transformer: 1:8 turns on OF47035 core
10) Resonant Capacitor: C_r =360nF /2222 383 20333 BC Components
11) Secondary and tertiary Diodes D_{S1} and D_{S2}: GUR5H60
12) Output Diodes: HFA16PA60C

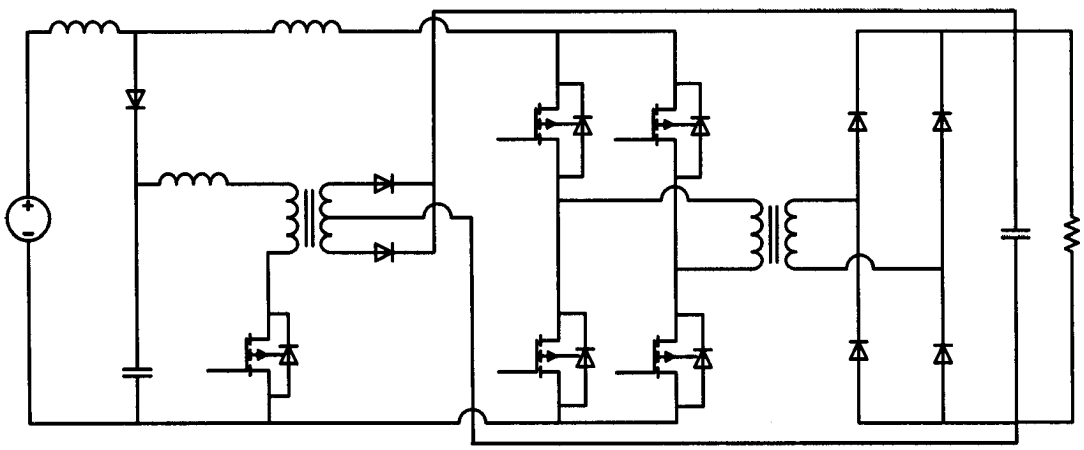

Fig.5.1 Experimental prototype boost converter circuit with the proposed Auxiliary circuit.

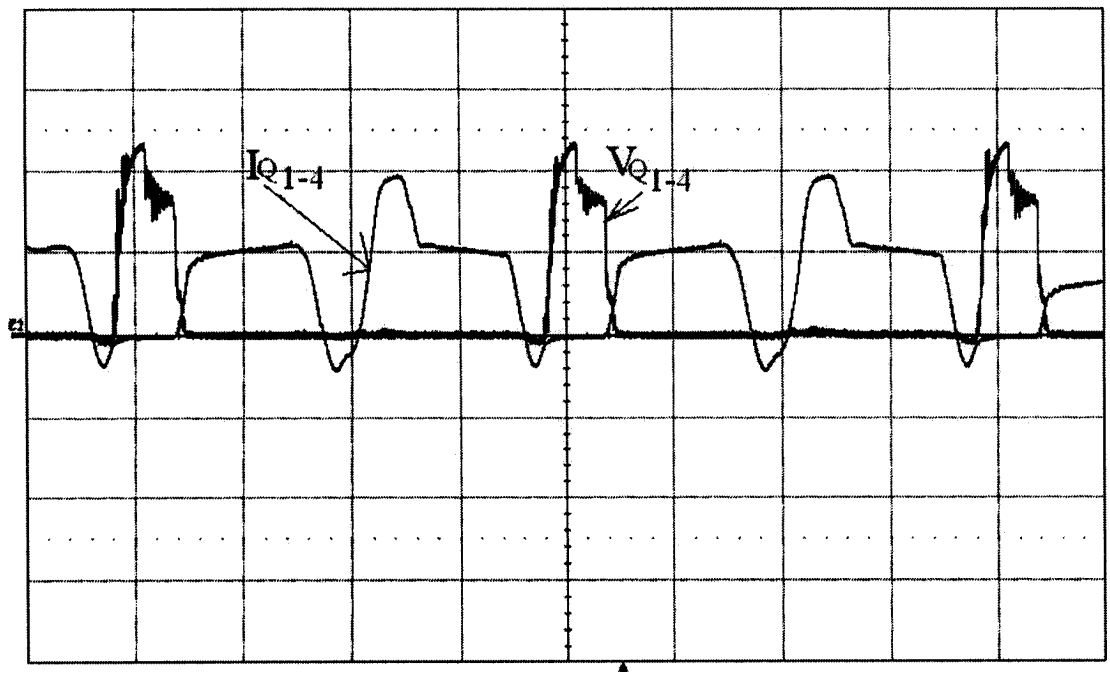

Fig.5.2 Main Switches $Q_{1\text{-}4}$ Current and Voltage waveforms:
(V: 30V/div, I: 15Amps/div, t:5μs/div)

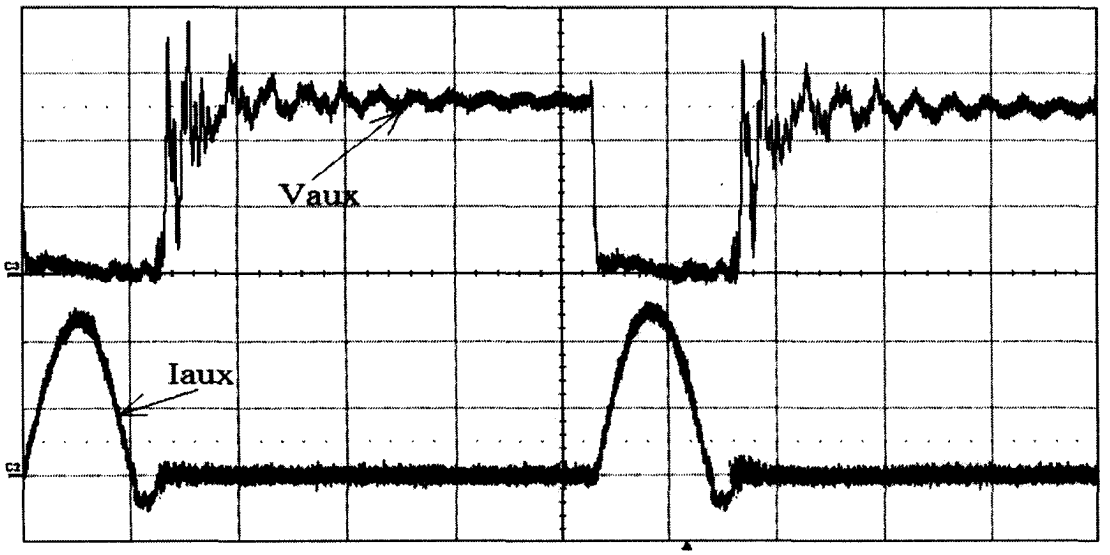

Fig. 5.3 Current and voltage in auxiliary switch over one switching period
(V: 30V/div, I: 15A/div, t:2 μs/div)

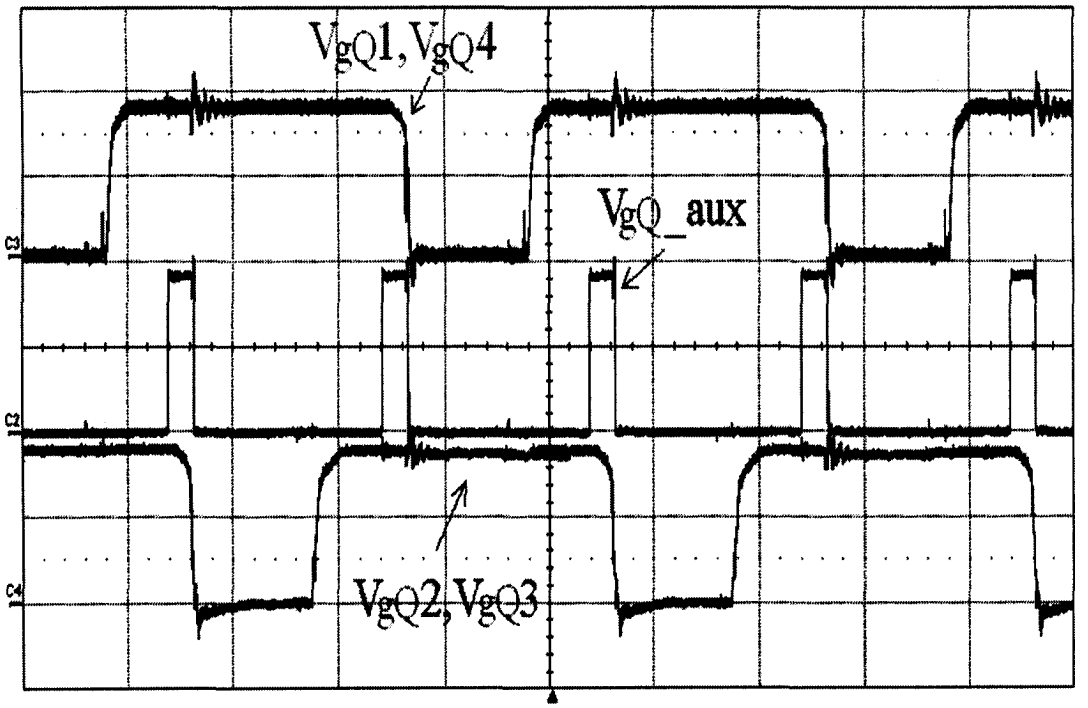

Fig.5.4 Gate pulses of the main and the auxiliary switches
(V: 10V/div, t: 5μs/div)

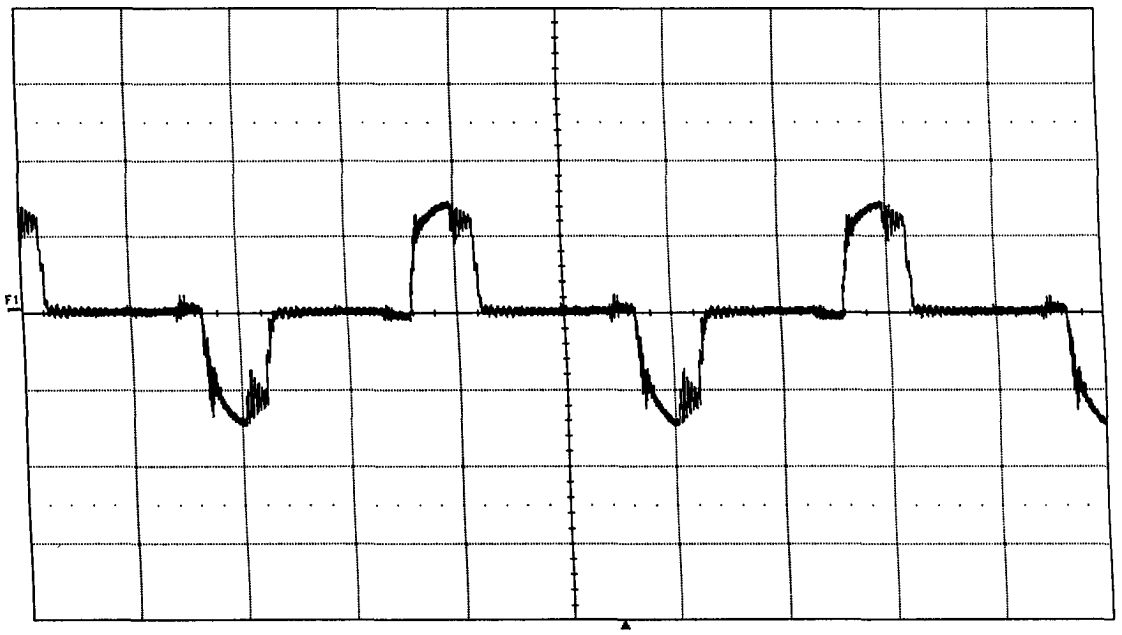

Fig.5.5 Transformer Primary Voltage Waveform (V: 50V.div, t:5 μs/div)

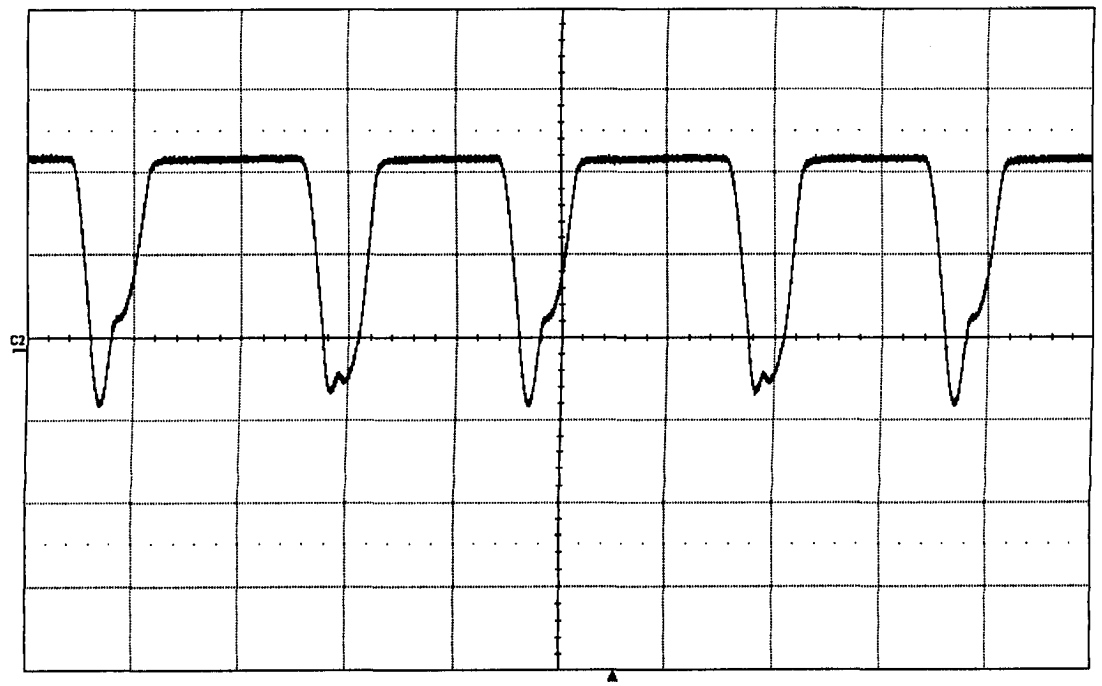

Fig.5.6 Bridge input current I_{Lr1} (I: 10A/div, t: 5 μs/div)

5.3 Conclusion from the Experimental Results

Fig 5.2 shows typical gating signals for the main switches Q_{1-4}. The auxiliary switch Q_{aux} voltage and current waveforms are shown in Fig 5.3. Gate pulses of the main and auxiliary switches are exposed in Fig5.4 and respectively main transformer primary voltage waveform and the bridge input current wave form are presented in Fig.5.5 and Fig.5.6 when P_o = 600W, V_{in} = 24V and f_{sw} = 50 kHz. The following observations can be made from the waveforms and graphs presented in Fig. 5.2 – 5.6:

(i) It can be seen from Fig 5.2 that the current through main switches Q_{1-4} goes negative before the switches are turned off and the voltage across the switches rises to the output voltage. The negative current that flows through switches Q_{1-4} before they turn off, implies that the current through the main switches is reversed and flows to their body diodes before the switches are turned off, thus showing that the switches undergo ZCS turn off. Also during turn-on, the current through the switches does not rise sharply rather the current through the main switch rises gradually and the voltage across it is zero when the current through it is rising. This shows that the main switches are turned on with ZCS. Also neither voltage nor current of the switches has any sharp high peaks.

(ii) It can be seen from Fig. 5.3 that the current in the auxiliary switch Q_{aux} also goes negative before it is turned off and voltage develops across it. This proves that the auxiliary circuit current is able to reduce to zero and

commutate the auxiliary switch current to its body diode before the switch is turned off hence ensuring ZCS turn off of the auxiliary switch. Also another point is the gradual rise of current in the auxiliary switch when it is turned on and its voltage drops to zero thus showing almost ZCS turn on of auxiliary switch.

(iii) From the graphs of the gate pulse waveforms in Fig.5.4, it can be seen that the auxiliary switch is activated for a very short duration compared to that of a full switching cycle, before a pair of main switches are turned-off.

(iv) It can be seen from Fig.5.5 that the primary voltage waveform is similar to that of a conventional current fed full-bridge converter and from fig.5.6 it can be seen that the negative current flowing in L_{r1} before it stops conducting altogether is fairly small. Since this small negative current is reverse-recovery current, the fact that it is small confirms that the auxiliary circuit can help minimize it.

5.4 Efficiency Results

Fig 5.7 shows the efficiency comparison of the new ZCS-PWM full-bridge boost converter and the conventional hard-switching PWM full-bridge boost converter. It can be seen that the PWM boost converter with the proposed auxiliary circuit (indicated as Efficiency of ZCS converter) has a significantly better efficiency than

the conventional PWM boost converter above 35% of the full load. The efficiency of the proposed PWM boost converter is consistently about 93%. The efficiency saving in ZCS- PWM in comparison with PWM hard switching is lower in low load than that in high load. The reason is that the sum of switching loss of the auxiliary and conduction loss of the auxiliary circuit is almost fixed. The fixed loss has a higher percentage in lower load than in higher load.

The efficiency improves because there is no turn-on or turn off switching losses of the main switches and also there is energy feed forward from the auxiliary circuit to the output. Normally, those two losses account for most of the switching loss of the conventional hard-switching PWM boost converter. Due to the ZCS turn-on and turn-off of the auxiliary switch, only minimal conduction losses that is introduced by the auxiliary switch is more than overcome by reduced switching losses and energy feed forward from the auxiliary circuit. On the other hand, the reverse recovery current is dramatically reduced by the auxiliary circuit, which also contributes in the efficiency improvement.

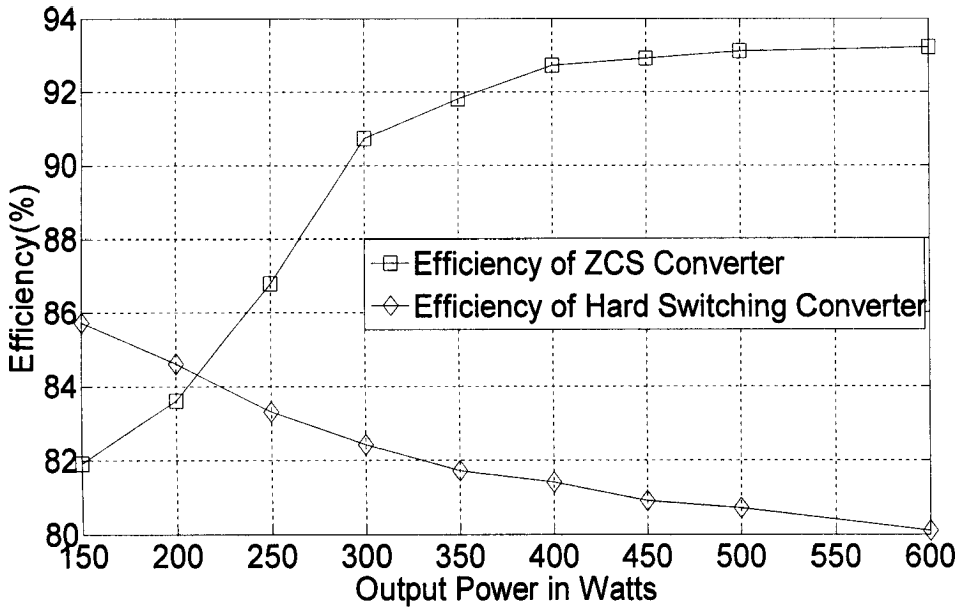

Fig.5.7. Efficiency measurements for the proposed converter and the conventional hard switching converter with 24V input and varying output load.

5.5 Conclusion

Experimental results confirming the feasibility of the proposed auxiliary circuit in a PWM full-bridge DC-DC boost converter were presented in this chapter. It was shown that the main converter switches and the auxiliary switch can operate with a ZCS turn-on and turn-off.

The efficiency of the converter operating with the proposed auxiliary circuit was compared to that of converter with no auxiliary circuit, which shows an increase of around 8% of overall maximum efficiency and hence justifies the use of such an auxiliary circuit in a DC-DC converter.

Chapter 6

Conclusion of the Thesis

6.1 Introduction

In this chapter, the contents of the thesis are summarized, the conclusions that have been reached as a result of the work performed in thesis are presented, and the main contributions of the thesis are stated. The chapter concludes by suggesting potential future research that can be done based on the thesis work.

6.2 Summary

The objective of this thesis was to propose, analyze, design, implement, and experimentally confirm the operation of a new ZCS-PWM dc-dc full-bridge boost converter that does not have the drawbacks of previously proposed circuits of the same type. In this thesis, the general operating principles of the converter were reviewed, and the converter's operation was discussed in detail and then analyzed mathematically. As a result of the mathematical analysis, key voltage and current equations that described the operation of the auxiliary circuit and other converter devices were derived. The steady state equations of each mode of operation were used as the basis of a MATLAB program that was used to generate steady-state characteristic curves that showed the effect that individual circuit parameters had on the operation of proposed auxiliary circuit and the boost converter.

Observations as to their steady-state characteristics were made and the curves were used as part of a design procedure to select the components of the converter, especially those of the auxiliary circuit. An experimental full-bridge PWM dc-dc boost converter prototype was built based on the converter design and typical waveforms were presented. The efficiency of the proposed converter operating with the auxiliary circuit was compared to that of a standard PWM dc-dc full-bridge boost converter and the increased efficiency of the proposed converter was confirmed.

6.3 Conclusion

The following conclusions can be made based on the results of this thesis:

(i) The efficiency of a PWM dc-dc full-bridge boost converter can be improved with the implementation of an auxiliary circuit that allows the converter switches to operate with ZCS.

(ii) It is possible to do so with fewer voltage and current component stresses than those found in other previously proposed ZCS dc-dc full-bridge converters.

(iii) The auxiliary circuit has several properties that should be considered when designing it to be implemented in the proposed converter, including the following

- The value of C_r, L_{r1} and the maximum input current can be used to fix the maximum voltage across the bridge switches, which is an unique property of the auxiliary circuit.

- Higher the value of C_r, lower will be the peak voltage across the bridge devices for a given value of maximum load current and L_{r1}.
- For L_{r2} and the auxiliary turns ratio of the transformer, higher the values of these components, lower will be maximum current stress on the auxiliary circuit.
- Higher values of C_r, L_{r1} and L_{r2} will increase the total activation time of the auxiliary circuit and the auxiliary switch, which is detrimental as this will increase conduction losses in the auxiliary circuit.

  As a result of these properties, a number of trade-offs need to be considered while choosing these components as discussed in the thesis.

6.4 Contributions

The principal contributions of this thesis are as follows:

(i) A new ZCS-PWM dc-dc full-bridge boost converter was proposed and its operation was explained.

(ii) The steady-state operation of the new converter was analyzed and a procedure for its design was derived. Based on the analysis and the design procedure, the general properties of the converter were established and were explained.

(iii) The feasibility and the properties of the new converter were experimentally confirmed by the implementation of a prototype. It was also confirmed that the

proposed converter is in fact more efficient that the conventional PWM dc-dc full-bridge boost converter for mid to full load conditions.

6.5 Proposal for Future Work

The following suggestions are made for future work:

(i) Single-switch PWM boost converters are widely used as ac-dc converters to improve input power factor. These converters take input ac voltage (usually typically from the utility) and convert it to a dc voltage, while simultaneously shaping the input current so that it is sinusoidal and in phase with the input voltage. Such a current maximizes the use of power from the utility and the act of shaping the current by using a boost converter is called power factor correction (PFC) in the literature. Since the proposed converter is a boost-type converter, it can be used as an ac-dc PFC converter and research can be done to see how well the proposed converter can operate in this particular application.

(ii) The proposed converter is a dc-dc converter with a large inductor connected to its full-bridge. As such, it can be considered to be a current source converter. Another type of current source converter that is widely used is a current source inverter or dc-ac converter. Given that the switches in an inverter operate differently than those of a dc-dc full-bridge converter and with higher voltages and currents, research can be done to see how the proposed converter can be adapted for use as a current source inverter.

(iii)The switches that were used in the proposed converter were low voltage MOSFETs. Research can be done to see how the converter would operate if it were implemented with other semiconductor devices with higher voltage and current ratings as switches such as thyristors, given the different properties of these devices.

Appendix:

1) MATLAB program for generating Characteristic Graphs in Fig.4.5 and Fig.4.6:

```
clc
 clear all
 V=40;
 Lr1=0.000013;
 Lr2=0.000009;
 Z=17;
 Cr=Lr2/(Z^2);
 w2=sqrt(1/(Lr2*Cr));
 L=Lr1*Lr2/(Lr1+Lr2);
 w=sqrt(1/(L*Cr));
 Z=sqrt(Lr2/Cr);
 X=(w2)^2;
 Y=w^2;
 i=1;
 t=0:0.00000005:0.0000018;

    I1= (400-V)/Z-((400-V)/Z)*(L/Lr2)*(1-cos(w*t))+V*(X/(Y*Lr2))*(t-
(sin(w*t))/w)-V*t/Lr2
    I2= 10.5-((400-V)/Z)*(L/Lr1)*(1-cos(w*t))+V*(X/(Y*Lr1))*(t-(sin(w*t))/w)


plot(t , I1,'b-')
hold on
plot(t,I2,'r')
grid on
xlabel('time')
ylabel('Current')
hold on
```

2) MATLAB program for generating Characteristic Graphs in Fig.4.3:

```
clc
 clear all
 V=80;
 i=1;
 j=1;
 for Lr = 0.000005:0.000001:0.000020
    LR(i)=Lr;
    i=i+1;
 end
 for Cr = 0.000000001:0.000000005:0.00000008
    CR(j)=Cr;
    Zo(j)= sqrt(LR(j)/Cr);
     Ip(j) = (400-V)/sqrt(LR(j)/CR(j));
    j=j+1;

 end

a=[Zo', Ip']
plot(Zo', Ip')
grid on
xlabel('Imp')
ylabel('Current')
hold on
```

3)MATLAB program for generating Characteristic Graphs in Fig.4.2:

```
clc
 clear all
 V=35;
 i=1;
 j=1;
 for Lr2 = 0.000001:0.000001:0.000010
    LR2(i)=Lr2;
    i=i+1;
 end
 for Lr1 = 0.000010:0.000001:0.000020
    LR1(j)=Lr1;
    r(j)= Lr2/Lr1;
     Ip(j) = (400-V)/sqrt(1+r(j))+400-V/(1+r(j));
    j=j+1;

 end

a=[r', Ip']
plot(r', Ip')
grid on
xlabel('Ratio of Lr2 and Lr1')
ylabel('Maximum Voltage across D1')
hold on
```

References:

[1] H. K. Yoon, S. K. Han, E. S. Choi, G. W. Moon, and M. J. Youn, "Zero-voltage switching and soft-commutating two-transformer full-bridge PWM Converter using the voltage-ripple," *IEEE Trans. Industrial Electronics*, vol.55, no.3, pp. 1478 – 1488, March 2008

[2] K. B. Park, C. E. Kim, G. W. Moon, and M. J. Youn "Voltage oscillation reduction technique for phase-shift full-bridge converter," *IEEE Trans. Industrial Electronics*, vol.54, no.5, pp. 2779 – 2790, Oct. 2007

[3] X. Wu, X. Xie, C. Zhao, Z. Qian, and R. Zhao "Low voltage and current stress ZVZCS full bridge DC–DC converter using center tapped rectifier reset," *IEEE Trans. Industrial Electronics*, vol. 55, no. 3, pp. 1470-1477, March 2008

[4] R. Watson and F. C. Lee, "A soft-switched, full-bridge boost converter employing an active- clamp circuit," in *Proc. IEEE PESC'96*, 1996, pp. 1948-1954.

[5] J. G. Cho, J. W. Baek, D. W. Yoo, D. I. Song, and G. H. Rim, "Zero-voltage-transition isolated PWM boost converter for single stage power factor correction," in *Proc. IEEE APEC'97*, 1997, pp. 471-476.

[6] J. Zhang, X. Xie, X. Wu, G. Wu, and Z. Qian, "A novel zero-current-transition full bridge DC/DC converter," *IEEE Trans. Power Electronics*, vol. 21, no.2, pp. 354 – 360, Mar. 2006.

[7] D. M. Xu, X. H. Wu, J. M. Zhang, and Z. Qian, "High power high frequency half-wave-mode ZCT-PWM full bridge DC/DC converter", in *Proc. IEEE APEC'00*, 2000, pp. 99 – 103.

[8] V. Yakushev, and S. Fraidlin, "Full-bridge isolated current fed converter with active clamp," in *Proc. IEEE APEC'99*, 1999, pp. 560 – 566.

[9] C. Qiao, and K. M. Smedley "An isolated full bridge boost converter with active soft switching," in *Proc. IEEE PESC'01*, 2001, pp. 896-903.

[10] L. Zhu, K. Wang, F.C. Lee, and J.-S. Lai "New start-up schemes for isolated full-bridge boost converters," *IEEE Trans. Power Electronics*, vol. 18, no.4, pp. 946 – 951, July 2003.

[11] C. Iannello, S. Luo, and I. Batarseh, "Full bridge ZCS PWM converter for high-voltage high-power applications," *IEEE Trans. Aerospace and Electronic Systems*, vol. 38, no.2, pp. 515 – 526, Apr. 2002.

[12] X. Zhu, D. Xu, H. Umida, K. Mino, and Z. Qian, "Current-fed phase shift controlled full bridge ZCS DC-DC converter with reverse block IGBT", in *Proc. IEEE APEC'06*, 2006, pp. 1605 – 1610.

[13] B. Su, and Z. Lu, "An improved single-stage power factor correction converter based on current-fed full- bridge topology," in *Proc. IEEE PESC'08*, 2008, pp. 472-475.

[14] S. W. Leung, S. H. Chung, and T. Chan, "A ZCS isolated full-bridge boost converter with multiple inputs," in *Proc. IEEE PESC'07,* 2007, pp. 2542 – 2548.

[15] Q.Sun, H.Wang, R. T. H. Li, H. S. H. Chung, S. Tapuchi, N. Huang, and A. Ioinovici "A ZCS full-bridge PWM converter with self-adaptable soft-switching snubber energy," in *Proc. IEEE PESC'08,* 2008, pp. 3001-3007.

[16] A. Averberg, K.R.Meyer, and A. Mertens, "Current-fed full bridge converter for fuel cell systems," in *Proc. IEEE PESC'08,* 2008, pp. 866-872.

[17] S. Jalbrzykowski and T. Citko, "Current-fed resonant full-bridge boost DC/AC/DC Converter," *IEEE Trans. Industrial Electronics,* vol. 55, no.3, pp.1198 – 1205, March 2008.

[18] J.-F. Chen, R.-Y. Chen, and T.-J. Liang, "Study and implementation of a single-stage current-fed boost PFC converter with ZCS for high voltage applications," *IEEE Trans. Power Electronics,* vol. 23, no.1, pp. 379-386, Jan. 2008.

[19] F. T. Wakabayashi, M. J. Bonato, and C. A. Canesin, "Novel high-power-factor ZCS-PWM preregulators," *IEEE Trans. Industrial Electronics,* vol. 48, no. 2, pp.322 – 333, April 2001.

[20] C. M. Wang, "A New Family of Zero-Current-Switching (ZCS) PWM Converters," *IEEE Trans. Industrial Electronics*, vol. 52, no. 4, pp. 1117 – 1125, Aug. 2005

[21] C. M. Wang, "New family of zero-current-switching PWM converters using a new zero-current-switching PWM auxiliary circuit," *IEEE Trans. Industrial Electronics*, vol 53, no. 3, pp. 768 – 777, June 2006.

[22] E. Adib, and H. Farzanehfard, "Family of zero-current transition PWM converters," *IEEE Trans. Industrial Electronics*, vol. 55, no. 8, pp. 3055 – 3063, Aug. 2008.

[23] C. M. Wang "A novel ZCS-PWM flyback converter with a simple ZCS-PWM commutation cell," *IEEE Trans. Industrial Electronics*, vol. 55, no. 2, pp. 749 – 757, Feb. 2008.

[24] D.-Y. Lee, M.-K. Lee, D.-S. Hyun, and I. Choy, "New zero-current-transition PWM DC/DC converters without current stress," *IEEE Trans. Power Electronics*, vol. 18, no.1, pp. 95-104, Apr. 2002.

[25] P. Das, and G. Moschopoulos, "A comparative study of zero-current-transition PWM converters," *IEEE Trans. Industrial Electronics*, vol. 54, no. 3, pp. 1319 – 1328, June 2007.

[26] P. Das, and G. Moschopoulos, "A zero-current-transition converter with reduced auxiliary circuit losses," *IEEE Trans. Power Electronics*, vol. 22, no.4, pp.1464 – 1471, July 2007